Eur. Phys. J. C 54, 517–538 (2008)
DOI 10.1140/epjc/s10052-008-0582-x

THE EUROPEAN PHYSICAL JOURNAL C

Regular Article – Experimental Physics

Quasielastic axial-vector mass from experiments on neutrino–nucleus scattering

K.S. Kuzmin[1,2,a], V.V. Lyubushkin[3,4,b], V.A. Naumov[1,c]

[1] Bogoliubov Laboratory of Theoretical Physics, Joint Institute for Nuclear Research, 141980 Dubna, Russia
[2] Institute for Theoretical and Experimental Physics, 117259 Moscow, Russia
[3] Dzhelepov Laboratory of Nuclear Problems, Joint Institute for Nuclear Research, 141980 Dubna, Russia
[4] Physics Department of Irkutsk State University, 664003 Irkutsk, Russia

Received: 29 December 2007 /
Published online: 3 April 2008 –

Abstract. We analyse available experimental data on the total and differential charged-current cross sections for quasielastic $\nu_\mu N$ and $\overline{\nu}_\mu N$ scattering, obtained with a variety of nuclear targets in the accelerator experiments at ANL, BNL, FNAL, CERN, and IHEP, dating from the end of sixties to the present day. The data are used to adjust the poorly known value of the axial-vector mass of the nucleon.

PACS. 13.15.+g; 25.30.Pt; 13.40.Gp

1 Introduction

A precise knowledge of the cross sections for charged-current induced quasielastic scattering (QES) of neutrinos and antineutrinos on nuclear targets is a pressing demand of the current and planning next generation experiments with accelerator and atmospheric neutrino beams, aiming at the further exploration of neutrino oscillations, probing nonstandard neutrino interactions, searches for proton decay, and related phenomena.

The quasielastic cross sections are very sensitive to the poorly known shape of the weak axial-vector form factor $F_{\mathrm{A}}(Q^2)$ of the nucleon. Adopting the conventional dipole approximation, this form factor is determined by the axial-vector coupling $g_{\mathrm{A}} = F_{\mathrm{A}}(0)$ and the phenomenological parameter M_{A}, the so-called axial-vector (dipole) mass related to the root-mean-square axial radius by

$$\left\langle r_{\mathrm{A}}^2 \right\rangle = -\frac{6}{g_{\mathrm{A}}} \left[\frac{\mathrm{d}F_{\mathrm{A}}(Q^2)}{\mathrm{d}Q^2} \right]_{Q^2=0} = \frac{12}{M_{\mathrm{A}}^2} \,.$$

The experimental values of M_{A} extracted from neutrino and antineutrino scattering data and from the more involved and vastly model-dependent analyses of charged pion electroproduction off protons, show very wide spread, from roughly 0.7 to 1.2 GeV with the formal weighted averages [1, 2]

$$M_{\mathrm{A}} = \begin{cases} 1.026 \pm 0.021\,\mathrm{GeV} & \text{from } \nu_\mu, \overline{\nu}_\mu \text{ experiments}\,, \\ 1.069 \pm 0.016\,\mathrm{GeV} & \text{from } \pi \text{ electroproduction}\,. \end{cases}$$

The first value, the common default in most current neutrino simulations, is defined largely by $\nu_\mu d$ bubble chamber experiments; in many of these experiments, the extractions of M_{A} were based on the naive dipole approximation for the vector form factors of the nucleon, along with other conjectures. The second value should be in fact decreased by about 5%, in order to account for hadronic loop corrections (see, e.g., [1]).

The results of several selected $\nu_\mu d$, $\overline{\nu}_\mu \mathrm{H}$, and $\pi^\pm$ electroproduction experiments have been recently reanalyzed by Bodek et al. [3], using a new improved description of the vector form factors ("BBBA(07)" parametrization). The obtained world average axial mass is

$$M_{\mathrm{A}} = 1.014 \pm 0.014\,\mathrm{GeV} \quad (\mathrm{BBBA(07)})\,.$$

This value seems to be in conflict with the new results of high-statistics neutrino experiments K2K SciFi [4] (oxygen target) and MiniBooNE [5] (carbon target), reported unexpectedly large while mutually consistent values of the axial mass:

$$M_{\mathrm{A}} = \begin{cases} 1.20 \pm 0.12\,\mathrm{GeV} & (\mathrm{K2K})\,, \\ 1.23 \pm 0.20\,\mathrm{GeV} & (\mathrm{MiniBooNE})\,. \end{cases}$$

A preliminary analysis of antineutrino data in MiniBooNE yields a consistent value of M_{A} [6].

Both K2K and MiniBooNE extractions utilize the *updated* vector form factors, from [7, 8] and [9], respectively. Within the low-Q^2 regions explored in K2K and MiniBooNE experiments, the difference between these parametrizations and BBBA(07) is comparatively small.

It can be noted that nuclear effects in the K2K analysis were accounted within the standard relativistic Fermi gas

[a] e-mail: KKuzmin@jinr.theor.ru
[b] e-mail: Vladimir.Lyubushkin@cern.ch
[c] e-mail: VNaumov@jinr.theor.ru

(RFG) model [10, 11], while the MiniBooNE analysis used RFG modified by including an "instrumental" free parameter κ which changes the strength of Pauli-blocking. A fit of the Q^2 shape above $0.25\,\mathrm{GeV}^2$ (where the variations of κ has no significant impact) leads to an even larger value of $M_\mathrm{A} = 1.25 \pm 0.12\,\mathrm{GeV}$.

In this study, which is in a sense complementary to that by Bodek et al. [3], we attempt to extract the axial mass value by a global statistical analysis of all available consistent data on the total and differential QES cross sections measured in accelerator experiments with ν_μ and $\overline{\nu}_\mu$ beams[1] from ANL [12–19], BNL [20–33], FNAL [34–40], CERN [41–64], and IHEP [65–74]. The detector media used in these experiments are hydrogen, deuterium, carbon, aluminium, argon, iron/steel, propane, freon, and also propane–freon and neon–hydrogen mixtures.

In the likelihood analysis, we use the most accurate phenomenological parametrizations for the vector form factors of the nucleon [75–77], we take into account all known sources of uncertainties, in particular, the systematic errors in the energy spectra of ν_μ and $\overline{\nu}_\mu$ beams. For description of nuclear effects we apply the standard RFG model. We examine possible difference between the values of M_A extracted from ν_μ and $\overline{\nu}_\mu$ data, and cross-check our results with the data on Q^2 distributions measured in several experiments.

2 Quasielastic neutrino scattering off free nucleon

2.1 Structure functions and cross section

Let us first summarize the well-known phenomenology for describing the hypercharge conserved quasielastic reactions on free nucleon targets

$$\begin{aligned} &\nu_\ell(k) + n(p) \to \ell^-(k') + p(p')\,, \\ &\overline{\nu}_\ell(k) + p(p) \to \ell^+(k') + n(p')\,. \end{aligned} \tag{1}$$

Here k, k', p, and p' denote the four-momenta and ℓ stays for e, μ, or τ. In this paper, we will neglect the proton–neutron mass difference,[2] since the resulting correction, in the $\nu_\mu/\overline{\nu}_\mu$ case, exclusively works near the reaction threshold and practically negligible for the energies of our current interest. The general formulas which take this effect into account, were derived in [78] (assuming T and C invariance) and in [79, 80] (avoiding these assumptions).

The double differential cross-section for these processes is a convolution of spin-averaged leptonic and hadronic tensors $L_{\alpha\beta}$ and $W_{\alpha\beta}$:

$$\frac{\mathrm{d}\sigma_\mathrm{free}}{\mathrm{d}E_\ell\,\mathrm{d}\cos\theta_\ell} = \frac{G_\mathrm{F}^2 P_\ell}{\pi(1+Q^2/M_W^2)^2}\left(\frac{L^{\alpha\beta}W_{\alpha\beta}}{4ME_\nu}\right). \tag{2}$$

[1] The ν_e, $\overline{\nu}_e$, ν_τ, and $\overline{\nu}_\tau$ beams from past and current accelerator experiments are not appropriate for measuring the QES cross sections.

[2] While our computer code operates with the most general formulas and relevant kinematics.

Here G_F is the Fermi coupling, $q = k - k'$ is the four-momentum transferred from the incoming (anti)neutrino to the nucleon, $Q^2 = -q^2$, M_W is the mass of intermediate W-boson; E_ν, E_ℓ, $P_\ell = \sqrt{E_\ell^2 - m_\ell^2}$, and θ_ℓ are, respectively, the incident (anti)neutrino energy, outgoing lepton energy, momentum, and scattering angle in the lab frame, m_ℓ is the lepton mass. The leptonic tensor defined by the product of the weak leptonic currents, is given by

$$L_{\alpha\beta}(k,k') = k'_\alpha k_\beta + k_\alpha k'_\beta - g_{\alpha\beta}(kk') \mp \mathrm{i}\varepsilon_{\alpha\beta\gamma\delta}k^\gamma k'^\delta\,, \tag{3}$$

where the upper (lower) sign is for ν_ℓ ($\overline{\nu}_\ell$). Assuming the isotopic invariance, the hadronic tensor is defined by the six structure functions $W_i(Q^2)$:

$$\begin{aligned} W_{\alpha\beta}(p,q) = &-g_{\alpha\beta}W_1 + \frac{p_\alpha p_\beta}{M^2}W_2 \\ &- \frac{\mathrm{i}\varepsilon_{\alpha\beta\gamma\delta}p^\gamma q^\delta}{2M^2}W_3 + \frac{q_\alpha q_\beta}{M^2}W_4 \\ &+ \frac{p_\alpha q_\beta + q_\alpha p_\beta}{2M^2}W_5 + \mathrm{i}\frac{p_\alpha q_\beta - q_\alpha p_\beta}{2M^2}W_6\,, \end{aligned} \tag{4}$$

where M is the mass of the "isoscalar" nucleon. Then combining (3) and (4) yields

$$\begin{aligned} \frac{L^{\alpha\beta}W_{\alpha\beta}}{4ME_\nu} = &\left(\frac{E_\ell - P_\ell\cos\theta_\ell}{M}\right)\left(W_1 + 2\kappa^2 W_4\right) \\ &\pm\left[\left(\frac{E_\nu + E_\ell}{M}\right)\left(\frac{E_\ell - P_\ell\cos\theta_\ell}{2M}\right) - 2\kappa^2\right]W_3 \\ &+ \frac{E_\ell + P_\ell\cos\theta_\ell}{2M}W_2 - 2\kappa^2 W_5\,, \end{aligned} \tag{5}$$

where $\kappa = m_\ell/2M$.

In order to connect the structure functions with the nucleon form factors, we define the charged hadronic current for the QES process (see, e.g., [81]):

$$\langle p(p')|J_\alpha|n(p)\rangle = V_{ud}\overline{u}_p(p')\Gamma_\alpha(p,q)u_n(p)\,. \tag{6}$$

Here V_{ud} is the ud transition element from the Cabibbo–Kobayashi–Maskawa quark-mixing matrix and

$$\begin{aligned} \Gamma_\alpha(p,q) = &\gamma_\alpha F_\mathrm{V} + \mathrm{i}\sigma_{\alpha\beta}\frac{q^\beta}{2M}F_\mathrm{M} + \frac{q_\alpha}{M}F_\mathrm{S} \\ &+ \left(\gamma_\alpha F_\mathrm{A} + \frac{p_\alpha + p'_\alpha}{M}F_\mathrm{T} + \frac{q_\alpha}{M}F_P\right)\gamma_5\,. \end{aligned} \tag{7}$$

The form factors F_i are in general complex functions of Q^2. After standard calculations one finds

$$W_i(Q^2) = 2M^2|V_{ud}|^2 w_i(Q^2)\delta\left(2(pq) - Q^2\right), \tag{8}$$

with

$$\begin{aligned} w_1 &= |F_\mathrm{A}|^2 + x'\left(|F_\mathrm{V} + F_\mathrm{M}|^2 + |F_\mathrm{A}|^2\right), \\ w_2 &= |F_\mathrm{V}|^2 + |F_\mathrm{A}|^2 + x'\left(|F_\mathrm{M}|^2 + 4|F_\mathrm{T}|^2\right), \\ w_3 &= -2\mathrm{Re}\left[F_\mathrm{A}^*(F_\mathrm{V} + F_\mathrm{M})\right], \end{aligned}$$

$$
\begin{aligned}
w_4 &= \frac{1}{4}\left[x'\left(|F_{\rm M}-2F_{\rm S}|+4|F_P+F_{\rm T}|^2\right)-|F_{\rm M}|^2\right] \\
&\quad +|F_{\rm S}|^2+\frac{1}{2}{\rm Re}\left[F_{\rm V}^*\left(2F_{\rm S}-F_{\rm M}\right)-2F_{\rm A}^*(F_P+F_{\rm T})\right], \\
w_5 &= w_2+2{\rm Re}\left[F_{\rm S}^*\left(F_{\rm V}-x'F_{\rm M}\right)-F_{\rm T}^*\left(F_{\rm A}-2x'F_P\right)\right], \\
w_6 &= 2{\rm Im}\left[F_{\rm S}^*\left(F_{\rm V}-x'F_{\rm M}\right)+F_{\rm T}^*\left(F_{\rm A}-2x'F_P\right)\right],
\end{aligned}
$$

and $x'=Q^2/4M^2$. The only difference between this result and that from [81] is in the relative sign of the terms in ω_6 which does not contribute to the QES cross section.[3]

Inserting (5) and (8) into (2) gives the commonly known formula for the differential cross section for reactions (1) on free nucleon targets:

$$
\begin{aligned}
\frac{{\rm d}\sigma_{\rm free}}{{\rm d}Q^2} &= \frac{G_{\rm F}^2M^2|V_{ud}|^2}{8\pi\left(1+Q^2/M_W^2\right)^2E_\nu^2} \\
&\quad\times\left[A\frac{m_\ell^2+Q^2}{M^2}+B\frac{s-u}{M^2}+C\frac{(s-u)^2}{M^4}\right],
\end{aligned}
$$

where

$$
\begin{aligned}
A &= 2x'|F_{\rm V}+F_{\rm M}|^2-(1+x')|F_{\rm V}|^2-x'(1+x')|F_{\rm M}|^2 \\
&\quad +(1+x')|F_{\rm A}|^2-4x'(1+x')|F_{\rm T}|^2 \\
&\quad -\kappa^2\left[|F_{\rm V}+F_{\rm M}|^2+|F_{\rm A}+2F_P|^2\right. \\
&\quad \left.-4(1+x')(|F_{\rm A}|^2+|F_P|^2)\right], \\
B &= \mp 4x'{\rm Re}\left[F_{\rm A}^*(F_{\rm V}+F_{\rm M})\right] \\
&\quad +4\kappa^2{\rm Re}\left[F_{\rm T}^*\left(F_{\rm A}-x'F_P\right)-F_{\rm S}^*\left(F_{\rm V}-x'F_{\rm M}\right)\right], \\
C &= \frac{1}{4}\left(|F_{\rm V}|^2+x'|F_{\rm M}|^2+|F_{\rm A}|^2+4x'|F_{\rm T}|^2\right), \\
s &= (k+p)^2=2ME_\nu+M^2, \\
u &= (k'-p)^2=m_\ell^2-2ME_\ell=m_\ell^2-2ME_\nu+Q^2.
\end{aligned}
$$

2.2 Induced scalar and tensor form factors

The quoted formulas take into account the nonstandard G parity violating axial and vector second-class currents (SCC) which induce the nonzero scalar and tensor form factors $F_{\rm S}$ and $F_{\rm T}$. The most robust restrictions on the SCC couplings $F_{\rm S,T}(0)$ come from the studies of β decay of complex nuclei (see, e.g., [82–85] and quoted therein references). However, these studies are almost insensitive to the SCC effects at nonzero Q^2. The latter were investigated in several (anti)neutrino experiments at BNL [25, 28–30] ($Q^2\lesssim 1.2\,{\rm GeV}^2$) and in the IHEP-ITEP spark chamber experiment at Serpukhov [71] ($Q^2\lesssim 2.4\,{\rm GeV}^2$), adopting the ad hoc dipole parameterizations

$$
\begin{aligned}
F_{\rm S}\left(Q^2\right) &= \xi_{\rm S}F_{\rm V}(0)\left(1+Q^2/M_{\rm S}^2\right)^{-2}, \\
F_{\rm T}\left(Q^2\right) &= \xi_{\rm T}F_{\rm A}(0)\left(1+Q^2/M_{\rm T}^2\right)^{-2}.
\end{aligned}
$$

[3] According to Llewellyn Smith, the functions $\omega_5'=\omega_5-\omega_2$ and ω_6 are, respectively, the real and imaginary parts of a unique function. Our examination does not confirm this property for the general case of nonvanishing second-class current induced form factors $F_{\rm S}$ and $F_{\rm T}$.

The strongest (but yet not too telling) 90% C.L. upper limit for the axial SCC strength $\xi_{\rm T}$ has been obtained at the BNL AGS $\overline{\nu}_\mu$ experiment [30] as a function of the "tensor mass" $M_{\rm T}$, assuming conservation of vector current (CVC) (that is $\xi_{\rm S}=0$), and simple dipole form for the vector and axial form factors with $M_{\rm V}=0.84\,{\rm GeV}$ and $M_{\rm A}=1.09\,{\rm GeV}$. The limit ranges between 0.78 at $M_{\rm T}=0.5\,{\rm GeV}$ to about 0.11 at $M_{\rm T}=1.5\,{\rm GeV}$. In so much as the contribution of the scalar form factor into the QES cross section is suppressed by $(m_\mu/M)^2\approx 0.01$, the 90% C.L. constraint to the vector SCC strength $\xi_{\rm S}$ is even less impressive: $\xi_{\rm S}<1.9$, assuming $\xi_{\rm T}=0$, $M_{\rm S}=1\,{\rm GeV}$, and the same $M_{\rm V}$ and $M_{\rm A}$ as above.

Below, keeping in mind this vagueness, we will assume the time and charge invariance of the hadronic current. Under this standard assumption, all the form factors are real functions of Q^2 and

$$
F_{\rm S}=F_{\rm T}=0\,.
$$

2.3 Vector form factors

The Dirac and Pauli form factors $F_{\rm V,M}$ are related to the Sachs electric and magnetic form factors $G_{\rm E,M}$:

$$
F_{\rm V}=\frac{G_{\rm E}+x'G_{\rm M}}{1+x'}\,,\quad F_{\rm M}=\frac{G_{\rm M}-G_{\rm E}}{1+x'}\,.
$$

Isotopic symmetry provides simple relation between $G_{\rm E,M}$ and elastic electric and magnetic form factors of proton and neutron $G_{\rm E}^{p,n}$ and $G_{\rm M}^{p,n}$:

$$
G_{\rm M}=G_{\rm M}^p-G_{\rm M}^n\,,\quad G_{\rm E}=G_{\rm E}^p-G_{\rm E}^n.
$$

At low Q^2, a reasonable description of the electric and magnetic form factors is given by the dipole approximation:

$$
G_{\rm E}^p\approx G_{\rm D}\,,\quad G_{\rm M}^p\approx\mu_pG_{\rm D}\,,\quad G_{\rm E}^n\approx 0\,,\quad G_{\rm M}^n\approx\mu_nG_{\rm D}\,,
$$

where $G_{\rm D}=(1+Q^2/M_{\rm V}^2)^{-2}$, $M_{\rm V}=0.84\,{\rm GeV}$, and μ_p (μ_n) is the anomalous magnetic moment of the proton (neutron). Analyses of the almost all earlier neutrino experiments were based on this approximation. In this study, we utilize two more sophisticated models for the form factors $G_{\rm E}^{p,n}$ and $G_{\rm M}^{p,n}$ – BBBA(07) [75, 76] and GKex(05)[77].

The BBBA(07) model is an accurate Kelly type parametrization of the current experimental data on the form factors $G_{\rm E}^p$, $G_{\rm M}^p$, $G_{\rm E}^n$, $G_{\rm M}^n$, and ratio $G_{\rm E}^p/G_{\rm M}^p$, which uses the Nachtmann scaling variable

$$
\xi_{p,n}=2\left(1+\sqrt{1+4M_{p,n}^2/Q^2}\right)^{-1},
$$

to relate elastic and inelastic form factors, and imposes quark–hadron duality asymptotic constraints at high momentum transfers where the quark structure dominates. The parametrization is based on the same datasets as were used by Kelly [86], updated to include some recent experimental results. Quark–hadron duality implies that the squared ratio of neutron and proton magnetic form factors

should be the same as the ratio of the corresponding inelastic structure functions F_2^n and F_2^p in the limit $\xi_{p,n} = 1$:

$$\left(\frac{G_{\rm M}^n}{G_{\rm M}^p}\right)^2 = \frac{F_2^n}{F_2^p} = \frac{1+4(d/u)}{4+(d/u)}\,, \quad Q^2 \to \infty\,.$$

Here d and u are the partonic density functions. The authors fit the data under the two assumptions: $d/u = 0$ and $d/u = 0.2$. One more duality-motivated constraint is the equality

$$(G_{\rm E}^n/G_{\rm M}^n)^2 = (G_{\rm E}^p/G_{\rm M}^p)^2$$

applied for the highest Q^2 data points for the neutron electric form factor included into the BBBA(07) fit.

The GKex(05) model is in fact a modification of the QCD inspired vector dominance model (VDM) by Gari and Krüempelmann (GK) [87, 88] extended and fine-tuned by Lomon [89, 90] in order to match the current and consistent earlier experimental data. The data set used by Lomon includes the polarization transfer measurements, which are directly related to the ratios of electric to magnetic form factors, and differential cross section measurements of the magnetic form factors. The electric form factors derived from the Rosenbluth separation of the differential cross section are only used for the lower range of Q^2 where the magnetic contributions are less dominant. Among several versions of the parametrization considered by Lomon, we chose the latest one "GKex(05)" described in [77]. This version incorporates the data that has become available since the publication [90] and has a bit better χ^2. The fitted parameters agree with the known constraints and the model is consistent with VDM at low Q^2, while approaching perturbative QCD behavior at high Q^2. The quark-hadron duality constraint is not imposed.

Figure 1 shows a comparison of the GKex(05) and BBBA(07) parametrizations for the form factors $G_{\rm E}^{p,n}$ and $G_{\rm M}^{p,n}$ divided by the standard dipole $G_{\rm D}$, against the experimental data extracted using either the Rosenbluth separation or polarization transfer techniques (including a series of double-polarization measurements of neutron knock-out from a polarized ^{2}H or ^{3}He targets). The data assemblage is borrowed from [91–94] and recent reviews [95, 96]. It is seen from the figure that the models are numerically close to each other at low momentum transfers covered by experiment, but diverge at high Q^2. The most serious disagreement between the models is in the neutron electric form factor at $Q^2 \gtrsim 2$ GeV^2. In Sect. 4, we examine how the model differences affect the extracted value of the axial mass.

2.4 Axial-vector and induced pseudoscalar form factors

For the axial and pseudoscalar form factors we use the conventional parametrizations [81]

$$F_{\rm A}(Q^2) = F_{\rm A}(0)\left(1+\frac{Q^2}{M_{\rm A}^2}\right)^{-2}, \qquad (9)$$

$$F_P(Q^2) = \frac{2M^2}{m_\pi^2+Q^2}F_{\rm A}(Q^2)\,, \qquad (10)$$

where $F_{\rm A}(0) = g_{\rm A}$ is the axial coupling, m_π is the charged pion mass, and $M_{\rm A}$ is the axial-vector mass treated as a free parameter. In fact, (10) is a conjecture inspired by the hypothesis of partial conservation of the axial current (PCAC), expectation that the form factor F_P is dominated by the pion pole near $Q^2 = 0$, and the "technical" condition

$$m_\pi^2\left|\frac{1}{F_{\rm A}(0)}\frac{{\rm d}F_{\rm A}(Q^2)}{{\rm d}Q^2}\right|_{Q^2=0} = \frac{2m_\pi^2}{M_{\rm A}^2} \ll 1\,,$$

which is obviously fulfilled for the experimental lower limit of $M_{\rm A}$. Since the pseudoscalar contribution enters into the cross sections multiplied by $(m_\ell/M)^2$, the uncertainty caused by this approximation may only be important for $\nu_\tau/\overline{\nu}_\tau$ induced reactions (especially in the low-Q^2 range, see, e.g., [97, 98]) and it is insignificant for reactions induced by electron and muon (anti)neutrinos.

2.5 Constants

The most precise determination of V_{ud} comes from superallowed nuclear beta decays ($0^+ \to 0^+$ transitions). We adopt the weighted average of the nine best measured superallowed decays $V_{ud}^{\rm (SA)} = 0.97377 \pm 0.00027$ recommended by the Particle Data Group (PDG) [99]. Note that this value is consistent with that of the PIBETA experiment at PSI [100], $V_{ud}^{\rm (PIBETA)} = 0.9728 \pm 0.0030$, obtained from the measured branching ratio for pion beta decay $\pi^+ \to \pi^0 e^+ \nu$.

For the axial-vector and Fermi coupling constants, we use the standard PDG averaged values: $g_{\rm A} = -1.2695 \pm 0.0029$ and $G_{\rm F} = 1.16637 \times 10^{-5}$ GeV^2 [99]. In several papers (see, e.g., [101] and references therein) it is suggested to use the value $G'_{\rm F} = 1.1803 \times 10^{-5}$ GeV^2 obtained from $0^+ \to 0^+$ nuclear β decays, rather than the standard $G_{\rm F}$ obtained from muon β decay. The coupling constant $G'_{\rm F}$ subsumes the bulk of the inner radiative corrections. However, some neutrino experiments already take the radiative corrections into account (sometimes in quite different ways) in the measured cross sections. That is why, in this study, we simply add the corresponding difference (of about 2%) to the overall uncertainty of the fit. Note that using the $G'_{\rm F}$ instead of $G_{\rm F}$ would lead to a few percent *decrease* of the output value of $M_{\rm A}$.

3 Relativistic Fermi gas model

Since the main part of the experimental data on the QES cross sections for nuclear targets was not corrected for nuclear effects, we must take these into account in our calculations. In the present work, we use the RFG model by Smith and Moniz [10, 11] incorporated as a standard tool into essentially all neutrino event generators employed in accelerator and astroparticle neutrino experiments.

According to RFG, the hadronic tensor $W_{\alpha\beta}$ given by (4) must be replaced with the tensor $T_{\alpha\beta}$, which describes the bound nucleon. This tensor is of the same Lorentz structure as $W_{\alpha\beta}$ and is defined by the six invari-

ant nuclear structure functions $T_i(Q^2)$. Thus, in the in the lab. frame

$$\begin{aligned} T_{\alpha\beta}\left(p_{\rm lab},q\right) &= -g_{\alpha\beta}T_1 + g_{0\alpha}g_{0\beta}T_2 \\ &\quad - \frac{i\varepsilon_{\alpha\beta 0\delta}q^{\delta}}{2M_t}T_3 + \frac{q_\alpha q_\beta}{M_t^2}T_4 \\ &\quad + \frac{g_{0\alpha}q_\beta + q_\alpha g_{0\beta}}{2M_t}T_5 \\ &\quad + \mathrm{i}\frac{g_{0\alpha}q_\beta - q_\alpha g_{0\beta}}{2M_t}T_6 \\ &= \int \mathrm{d}\mathbf{p} f(\mathbf{p},\mathbf{q}) W_{\alpha\beta}(p,q)\,, \end{aligned} \tag{11}$$

where $p_{\rm lab} = (M_t, \mathbf{0})$, M_t is the mass of the target nucleus, and

$$f(\mathbf{p},\mathbf{q}) = v_{\rm rel}^{-1}\overline{n}_i(\mathbf{p})\left[1 - n_f(\mathbf{p}+\mathbf{q})\right].$$

The function $\overline{n}_i(\mathbf{p})$ is the Fermi momentum distribution of the target nucleons, satisfying the normalization condition

$$\int \overline{n}_i(\mathbf{p})\,\mathrm{d}\mathbf{p} = 1\,.$$

The factor $1 - n_f(\mathbf{p}+\mathbf{q})$ (the unoccupation probability) takes into account the Pauli blocking for the outgoing nucleon. The relative velocity $v_{\rm rel}$ which represents the flux of incident particles, is given by

$$v_{\rm rel} = |(kp)|/(E_\nu M_t)\,.$$

Explicitly defining the three-momenta $\mathbf{q}$, $\mathbf{p}$, and $\mathbf{p}$,

$$\begin{aligned} \mathbf{q} &= (0,0,|\mathbf{q}|)\,, \\ \mathbf{p} &= (\sin\theta_{\mathbf{k}}, 0, \cos\theta_{\mathbf{k}})\,|\mathbf{q}|\,, \\ \mathbf{p} &= (\sin\theta_{\mathbf{p}}\cos\phi_{\mathbf{p}}, \sin\theta_{\mathbf{p}}\sin\phi_{\mathbf{p}}, \cos\theta_{\mathbf{p}})\,|\mathbf{p}|\,, \end{aligned}$$

one obtains

$$v_{\rm rel} = \left[E_{\mathbf{p}} - |\mathbf{p}|\left(\cos\theta_{\mathbf{k}}\cos\theta_{\mathbf{p}} + \sin\theta_{\mathbf{k}}\sin\theta_{\mathbf{p}}\sin\varphi_{\mathbf{p}}\right)\right]/M_t\,,$$

where

$$E_{\mathbf{p}} = \sqrt{\mathbf{p}^2 + M^2} - \epsilon_{\rm b}$$

is the total energy of the bound nucleon and $\epsilon_{\rm b}$ is the effective binding energy. The angle $\theta_{\mathbf{k}}$ is defined by

$$\cos\theta_{\mathbf{k}} = \frac{E_\nu^2 + \mathbf{q}^2 + m_\ell^2}{2E_\nu|\mathbf{q}|}\,.$$

For determining the angle $\theta_{\mathbf{p}}$, one can use the energy conservation law defined by delta-function

$$\delta(E_{\mathbf{p}} - E_{\mathbf{p}+\mathbf{q}} + \nu) = \frac{1}{2|\mathbf{p}||\mathbf{q}|}\delta\left(\cos\theta_{\mathbf{p}} - \cos\theta_{\mathbf{p}}^0\right),$$

where $\nu = E_\nu - E_\ell$ and

$$E_{\mathbf{p}+\mathbf{q}} = \sqrt{\mathbf{p}^2 + \mathbf{q}^2 + 2|\mathbf{p}||\mathbf{q}|\cos\theta_{\mathbf{p}} + M^2}\,.$$

is the total energy of the outgoing nucleon. Then the condition

$$\cos\theta_{\mathbf{p}} = \cos\theta_{\mathbf{p}}^0 = \frac{(\nu + E_{\mathbf{p}})^2 - (E_{\mathbf{p}} + \epsilon_{\rm b})^2 - \mathbf{q}^2}{2|\mathbf{p}||\mathbf{q}|}$$

must be obeyed.

The nuclear structure functions are the linear combination of the W_i and can be straightforwardly calculated from (4) and (11):

$$\begin{aligned} T_1 &= a_1 W_1 + \frac{1}{2}\left(a_2 - a_3\right)W_2\,, \\ T_2 &= \left[\frac{\mathbf{q}^2 - \nu^2}{2\mathbf{q}^2}\left(a_2 - a_3\right) + \frac{\nu^2}{\mathbf{q}^2}a_3 + a_4 - \frac{2\nu}{|\mathbf{q}|}a_5\right]W_2\,, \\ T_3 &= \frac{M_t}{M}\left(a_7 - \frac{\nu}{|\mathbf{q}|}a_6\right)W_3\,, \\ T_4 &= \frac{M_t^2}{M^2}\left[\frac{M^2}{2\mathbf{q}^2}\left(3a_3 - a_2\right)W_2 + a_1 W_4 + \frac{M}{|\mathbf{q}|}a_6 W_5\right], \\ T_5 &= \frac{M_t}{|\mathbf{q}|}\left[\frac{\nu}{|\mathbf{q}|}\left(a_2 - 3a_3\right) + 2a_5\right]W_2 \\ &\quad + \frac{M_t}{M}\left(a_7 - \frac{\nu}{|\mathbf{q}|}a_6\right)W_5\,, \\ T_6 &= \frac{M_t}{M}\left(a_7 - \frac{\nu}{|\mathbf{q}|}a_6\right)W_6\,. \end{aligned}$$

The coefficients a_i are given by

$$\begin{aligned} a_1 &= \int f(\mathbf{p},\mathbf{q})\,\mathrm{d}\mathbf{p}\,, \\ a_2 &= \frac{1}{M^2}\int f(\mathbf{p},\mathbf{q})\mathbf{p}^2\,\mathrm{d}\mathbf{p}\,, \\ a_3 &= \frac{1}{M^2}\int f(\mathbf{p},\mathbf{q})\mathbf{p}^2\cos^2\theta_{\mathbf{p}}\,\mathrm{d}\mathbf{p}\,, \\ a_4 &= \frac{1}{M^2}\int f(\mathbf{p},\mathbf{q})E_{\mathbf{p}}^2\,\mathrm{d}\mathbf{p}\,, \\ a_5 &= \frac{1}{M^2}\int f(\mathbf{p},\mathbf{q})E_{\mathbf{p}}|\mathbf{p}|\cos\theta_{\mathbf{p}}\,\mathrm{d}\mathbf{p}\,, \\ a_6 &= \frac{1}{M}\int f(\mathbf{p},\mathbf{q})|\mathbf{p}|\cos\theta_{\mathbf{p}}\,\mathrm{d}\mathbf{p}\,, \end{aligned}$$

Table 1. Proton and neutron Fermi momenta and binding energies (in MeV) for selected nuclei

Nucleus	$p_{\rm F}^p$	$\epsilon_{\rm b}^p$	$p_{\rm F}^n$	$\epsilon_{\rm b}^n$
$^{12}_{6}$C	221	25.6	221	25.6
$^{14}_{7}$N	223	26.2	223	26.1
$^{16}_{8}$O	225	26.6	225	26.6
$^{19}_{9}$F	233	28.4	233	28.3
$^{20}_{10}$Ne	230	27.8	230	27.8
$^{27}_{13}$Al	239	29.5	239	29.4
$^{40}_{18}$Ar	242	30.7	259	35.0
$^{56}_{26}$Fe	251	33.0	263	36.1
$^{80}_{35}$Br	245	31.5	270	38.1

$$a_7 = \frac{1}{M}\int f(\mathbf{p},\mathbf{q})E_{\mathbf{p}}\,\mathrm{d}\mathbf{p}\,.$$

Finally, in order to describe the neutrino scattering off a bound nucleon, one should substitute $M \longmapsto M_t$ and $W_i \longmapsto T_i$ in (5); then the differential cross-section can be calculated according to (2) (see [64] for more details). Table 1 collects the values of proton and neutron Fermi momenta $p_{\mathrm{F}}^{p,n}$ and binding energies $\epsilon_{\mathrm{b}}^{p,n}$ for several nuclei, used in our numerical calculations.

4 Statistical analysis of the data

4.1 Description of experimental data

We have examined and classified all available experimental data on quasielastic scattering with $\Delta Y = 0$. Published results from the relevant experiments with ν_μ and $\overline{\nu}_\mu$ beams from accelerators at ANL [12–19], BNL [20–33], FNAL [34–40], CERN [41–64], and IHEP [65–74] are included dating from the end of sixties to the present day, covering a variety of nuclear targets, with energies ranging from about 150 MeV (ANL experiments) to about 350 GeV (NuTeV). Pertinent additional information was borrowed from the review articles and data compilations [102–116].

All the fits are done with the CERN function minimization and error analysis package "MINUIT" (version 94.1) [117, 118], taking care of getting an accurate error matrix. The errors of the output parameters quoted below correspond to the usual one-standard-deviation (1σ) errors (MINUIT default).

For the analysis, we have selected the most statistically reliable measurements of the total and differential cross sections for each nuclear target, which were not superseded or reconsidered (due to increased statistics, revised normalization, etc.) in the posterior reports of the same experimental groups. Finally, we include into the global fit the data on the total cross sections from [18, 24, 25, 35, 39, 40, 43, 53, 58, 63, 64, 71, 74] and the data for the differential cross sections from [53, 60, 67, 68, 71, 74, 108]. The remaining data are either obsolete, or exhibit uncontrollable systematic errors and/or fall well outside the most probable range determined through the fit of the *full* dataset; the value of χ^2 evaluated for each subset of the rejected data usually exceeds $(3-4)$ NDF.

Since the differential cross sections $\mathrm{d}\sigma/\mathrm{d}Q^2$ were measured, as a rule, within rather wide ranges of the energy spectra of ν_μ and $\overline{\nu}_\mu$ beams, we use only the data from such

Table 2. Values of M_{A} (given in GeV), extracted by fitting the ν_μ, $\overline{\nu}_\mu$, and $\nu_\mu + \overline{\nu}_\mu$ data on total and differential QES cross sections, using the BBBA(07) and GKex(05) models for the vector form factors of the nucleon. The χ^2/NDF values for each fit are shown in parentheses

BBBA(07)			GKex(05)		
M_{A}^{ν}	$M_{\mathrm{A}}^{\overline{\nu}}$	$M_{\mathrm{A}}^{\nu+\overline{\nu}}$	M_{A}^{ν}	$M_{\mathrm{A}}^{\overline{\nu}}$	$M_{\mathrm{A}}^{\nu,\overline{\nu}}$
Fit to the total cross sections:					
0.994 ± 0.017	1.047 ± 0.025	1.011 ± 0.014	0.986 ± 0.017	1.035 ± 0.025	1.001 ± 0.014
(83/82)	(134/62)	(220/145)	(83/82)	(137/62)	(222/145)
Fit to the differential cross sections:					
0.979 ± 0.020	0.991 ± 0.029	0.983 ± 0.017	0.976 ± 0.020	0.982 ± 0.030	0.978 ± 0.017
(45/48)	(26/37)	(71/86)	(45/48)	(25/37)	(70/86)
Fit to the total and differential cross sections:					
0.988 ± 0.013	1.023 ± 0.018	0.999 ± 0.011	0.981 ± 0.013	1.012 ± 0.019	0.991 ± 0.011
(128/131)	(163/100)	(293/232)	(128/131)	(163/100)	(293/232)

Table 3. The same as in Table 2 but after exclusion of the datasets from experiments with non-active targets (NuTeV 1984 [40], IHEP-ITEP 1981,82,85 [66, 68, 71]) and the lowest-energy data of CERN 1967 [43] (see text for details)

BBBA(07)			GKex(05)		
M_{A}^{ν}	$M_{\mathrm{A}}^{\overline{\nu}}$	$M_{\mathrm{A}}^{\nu+\overline{\nu}}$	M_{A}^{ν}	$M_{\mathrm{A}}^{\overline{\nu}}$	$M_{\mathrm{A}}^{\nu,\overline{\nu}}$
Fit to the total cross sections:					
0.986 ± 0.021	0.855 ± 0.046	0.958 ± 0.019	0.977 ± 0.021	0.837 ± 0.046	0.948 ± 0.019
(42/52)	(38/35)	(88/88)	(42/52)	(38/35)	(89/88)
Fit to the differential cross sections:					
0.966 ± 0.024	0.971 ± 0.042	0.967 ± 0.021	0.963 ± 0.024	0.959 ± 0.043	0.962 ± 0.021
(33/33)	(16/22)	(49/56)	(34/33)	(15/22)	(49/56)
Fit to the total and differential cross sections:					
0.977 ± 0.016	0.912 ± 0.030	0.962 ± 0.014	0.971 ± 0.016	0.896 ± 0.031	0.954 ± 0.014
(75/86)	(58/58)	(137/145)	(76/86)	(57/58)	(138/145)

experiments, in which the spectra were known (measured or calculated and then calibrated) with reasonably good accuracy. All the energy spectra (borrowed from [53, 59, 71, 108, 111, 119, 120]) necessary for numerical averaging of the calculated differential cross sections and distributions were parametrized. To avoid the loss of accuracy, the precision of these parametrizations was chosen to be at least an order of magnitude better than the experimental accuracy of the spectra themselves. For a verification, we have estimated the mean energies of the beams for different energy intervals, and have compared these against the published values.

The analyses were performed for neutrino and antineutrino data separately, and for the full set of the ν and $\overline{\nu}$ data together. For each fit, we have included the data for either total or differential cross sections, as well as for the cross sections of both types together. The main results of the analysis are summarised in Tables 2 and 3 and illustrated in Figs. 2–15. Let us discuss these results in details.

4.2 Main results of the global fit

As is seen from Table 2, the differences between the values of $M_{\rm A}$ extracted from the fits of each type, performed with the BBBA(07) and GKex(05) models for the vector form factors vary between 0.3% and 1.3% that is less than or of the order of one standard deviation in the $M_{\rm A}$ extrac-

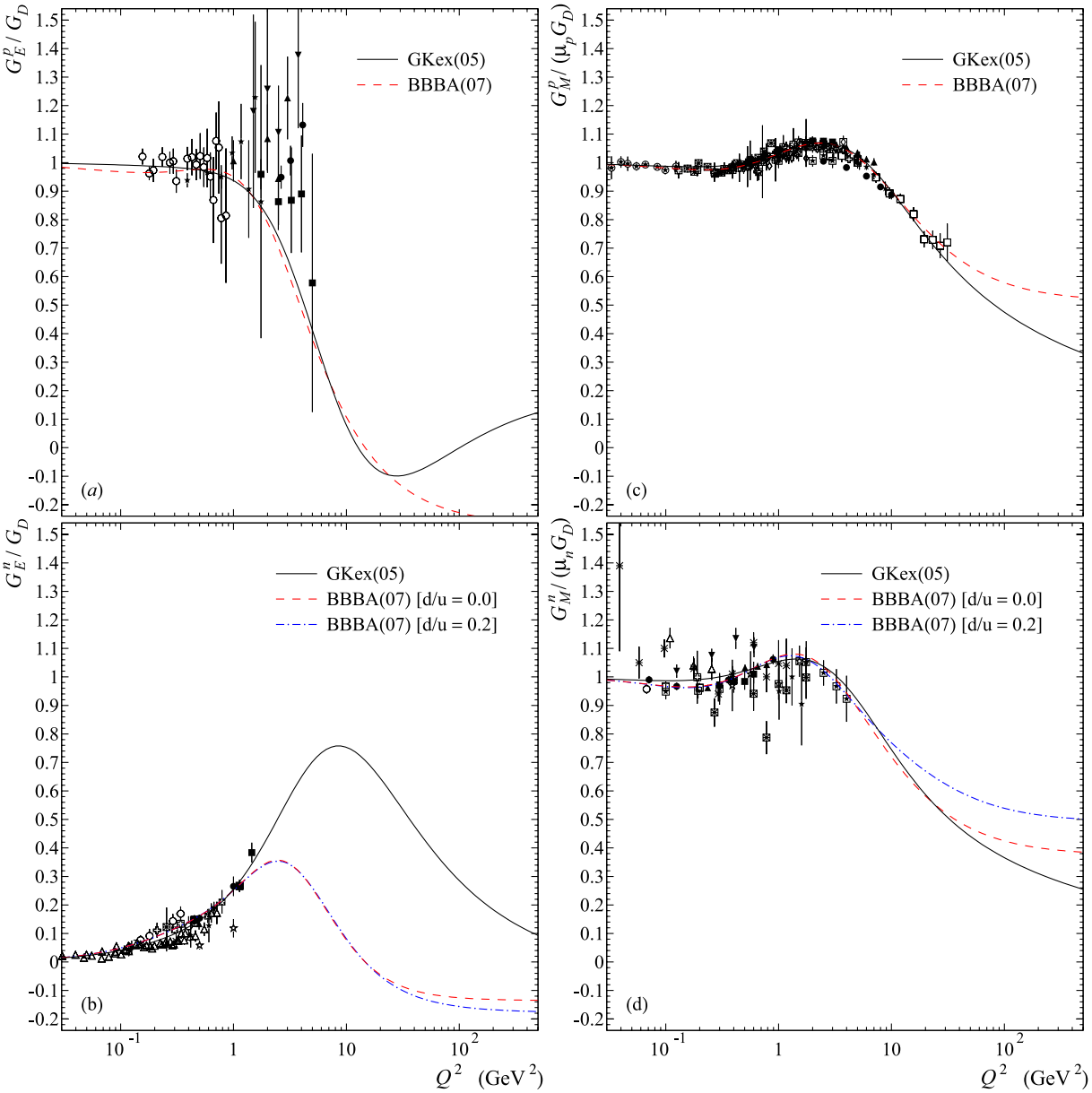

Fig. 1. Comparison of the GKex(05) and BBBA(07) models for the electric and magnetic form factors of proton and neutron (divided by the standard dipole $G_{\rm D}$) with the data from electron scattering experiments. The data compilation is taken from [91–96]. The two versions of the BBBA(07) parametrization are shown for the neutron form factors

tions and is comparable with the accuracy of the most precise measurements of the electric and magnetic form factors. The values of χ^2/NDF are essentially the same for BBBA(07) and GKex(05). The differences in the M_A values obtained with the two versions of the BBBA(07) model corresponding to $d/u = 0$ and 0.2 (the latter is not shown in the table) are less than 0.2% that is practically negligible. Therefore, in the following we will solely discuss the $d/u = 0$ case.

The M_A values obtained from the fits to the differential cross sections are systematically lower those obtained from the total cross sections. The differences amount $\sim 1.5\%$ ($\sim 5.7\%$) for ν_μ ($\overline{\nu}_\mu$) that is (especially in antineutrino case) above the statistical error of the fit and is caused

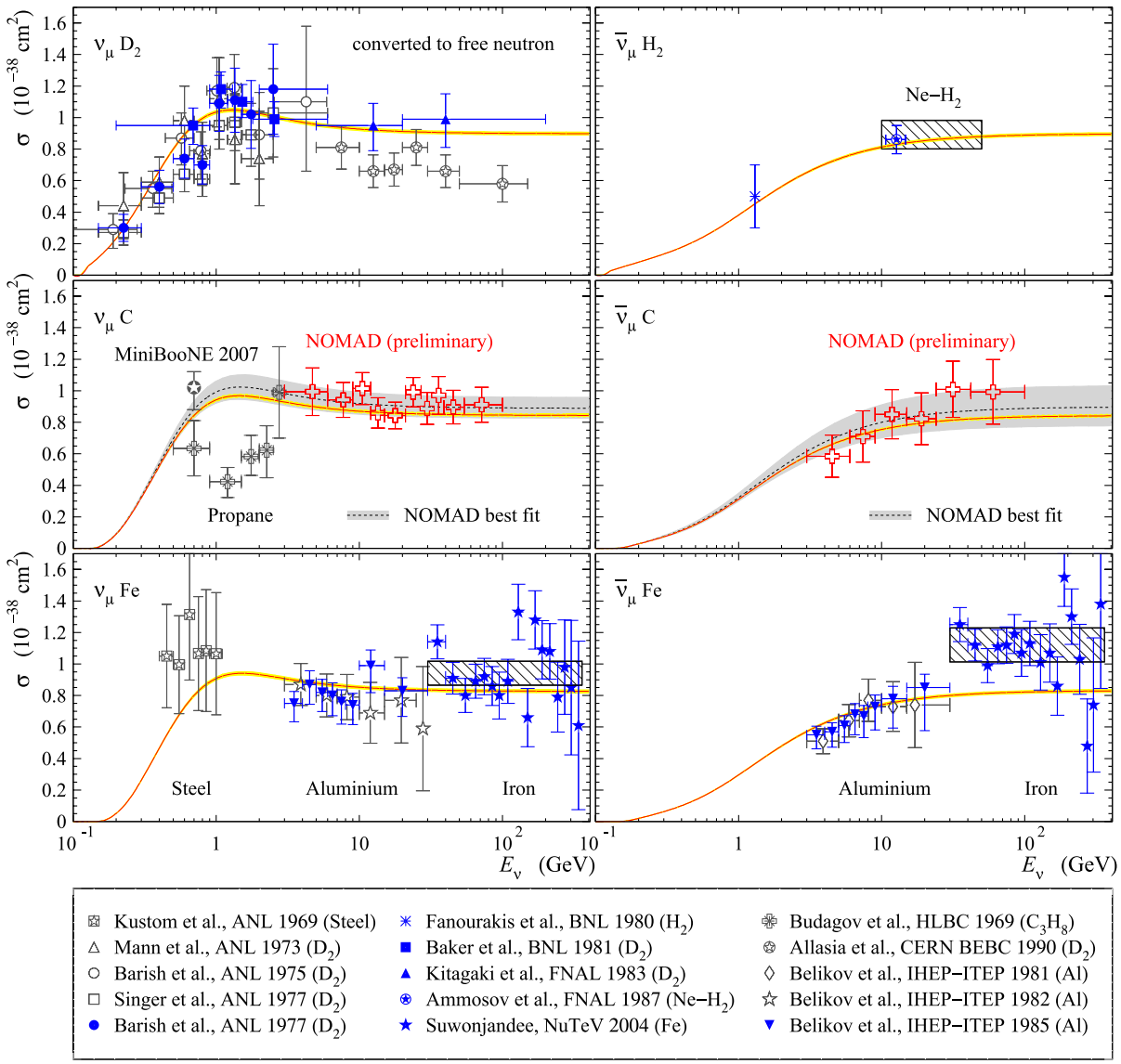

Fig. 2. Total quasielastic $\nu_\mu n$ and $\overline{\nu}_\mu p$ cross sections measured in experiments with deuterium, hydrogen, carbon/propane, aluminium, and iron/steel targets at ANL 1969 [13], ANL 1973 [15], ANL 1975 [16], ANL 1977 [17, 18], BNL 1980 [24], BNL 1981 [25], FNAL 1983 [35], FNAL E180 1984 [36, 37] (*rectangle* in top right panel), FNAL E180 1987 [39], NuTeV 2004 [40] (points and *rectangles* in bottom panels), CERN HLBC 1969 [46], CERN BEBC 1990 [60] (*points* and *rectangle* in top left panel), CERN NOMAD 2008 [64] (preliminary), IHEP-ITEP 1981 [66], IHEP-ITEP 1982 [68], and IHEP-ITEP 1985 [70, 71]. The deuterium and neon-hydrogen data were converted to a free neutron/proton target by the authors of the experiments. The MiniBooNE 2007 point [5] recalculated from the reported value of $M_A = 1.23 \pm 0.20$ GeV is also shown for comparison. The error bars represent the total errors which include the flux normalization uncertainties. The *solid curves* and *narrow shaded bands* are calculated with the BBBA(07) model for the vector form factors, with $M_A = 0.999 \pm 0.011$ GeV, the value obtained from the global fit to a subset of the full data set of total and differential cross sections (233 data points). The *points* shown by *grey symbols* are excluded from the fit, being either superseded by newer experiments, or not satisfying our selection criteria. The *dashed curves* and corresponding bands are the cross sections obtained by fitting the NOMAD 2008 alone with the GKex(2005) vector form factors (separately for ν_μ and $\overline{\nu}_\mu$ data)

mainly by uncertainties in the energy spectra of ν_μ and $\overline{\nu}_\mu$ and, in lesser extent, in the nuclear effects.

Figures 2 and 3 show a compilation of the available data on the total QES cross sections for the following nuclear targets: hydrogen [24], deuterium [15–18, 25, 35, 60], carbon [64], aluminium [66, 68, 70, 71], argon [63], iron [40], steel [13], propane [46], freon [43, 48, 51, 53, 65, 73, 74, 111], and also propane–freon [55, 58, 59] and neon–hydrogen [36, 37, 39] mixtures. The recent MiniBooNE 2007 datapoint [5] (carbon target) estimated from the reported value of M_A is also shown in Fig. 2 for comparison.

The compilation does not include obviously obsolete data (e.g., ANL 1972 [14], CERN HLBC 1965/1966 [41, 42]), as well as the data identical to those reported in the posterior publications of the same experimental groups (e.g., FNAL 1982 [34], GGM 1978 [56], IHEP-ITEP 1983 [69], IHEP SKAT 1986 [72]). The early results of the NOMAD experiment reported in [61, 62], have been considerably revised (mainly due to corrections in nuclear Monte Carlo) [64]; the datapoints shown in Fig. 2 are still *preliminary* and are reproduced here by permission of the NOMAD Collaboration.

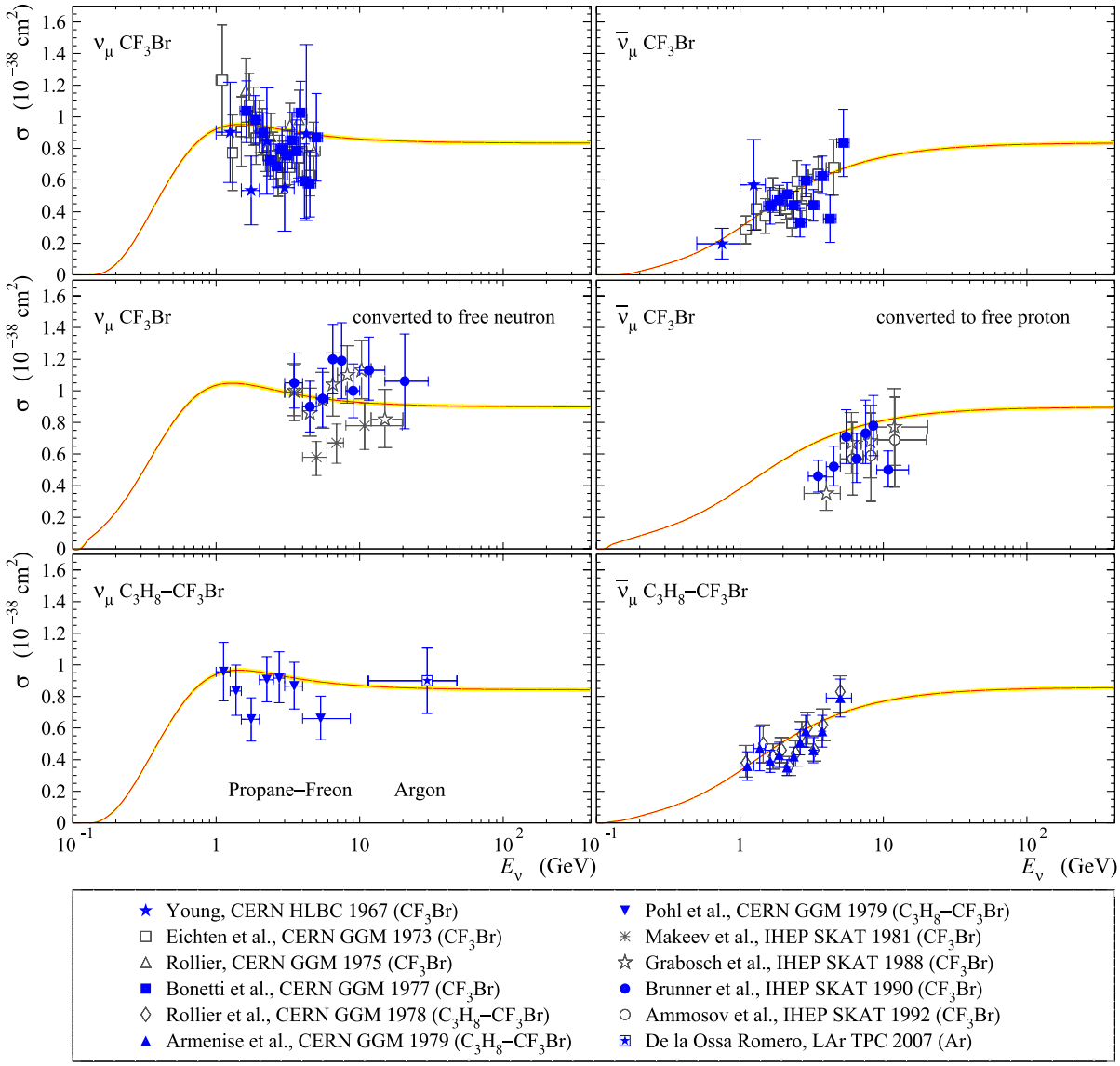

Fig. 3. Total quasielastic $\nu_\mu n$ and $\overline{\nu}_\mu p$ cross sections measured with the freon and propane-freon filled bubble chamber experiments CERN HLBC 1966 [42], CERN HLBC 1967 [43], CERN GGM 1973 [48], CERN GGM 1975 [51, 104], CERN GGM 1977 [53], CERN GGM 1978 [55], CERN GGM 1979 [58, 59], IHEP SKAT 1981 [65], IHEP SKAT 1988 [73], IHEP SKAT 1990 [74], and IHEP SKAT 1992 [111]. The point recently obtained in experiment with the liquid argon time projection chamber (LAr TPC 2007) [63] is also shown. The SKAT datapoints were converted from freon to a free neutron/proton target by the authors of the experiments. The error bars represent the total errors which include the uncertainties due to flux normalization and nuclear Monte Carlo. The *solid curves* and *narrow shaded bands* are calculated with the BBBA(07) model for the vector form factors, with the global fit value of $M_A = 0.999 \pm 0.011$ GeV. See caption of Fig. 2 for more details

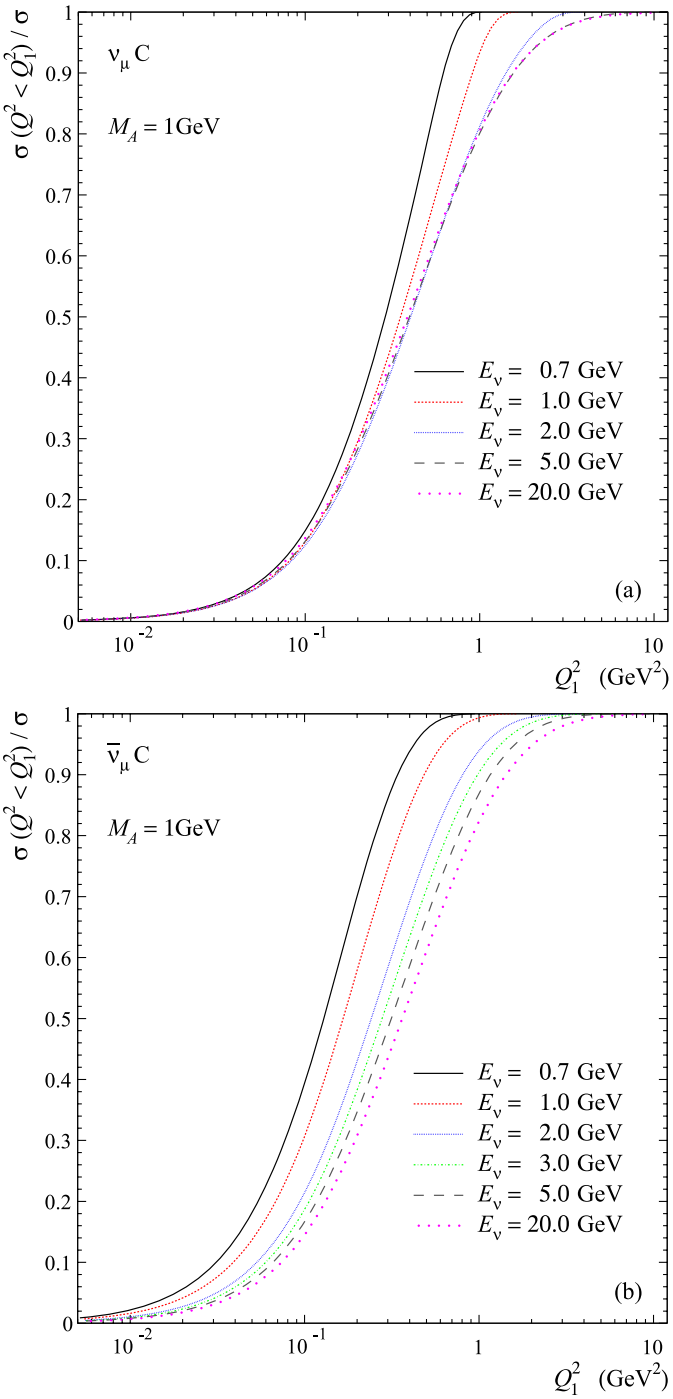

Fig. 4. The ratio $R = \sigma\left(Q^2 < Q_1^2\right)/\sigma$ vs. Q_1^2, evaluated for ν_μ and $\overline{\nu}_\nu$ quasielastic interactions with carbon target at several (anti)neutrino energies. The $M_{\rm A}$ value is taken to be 1 GeV

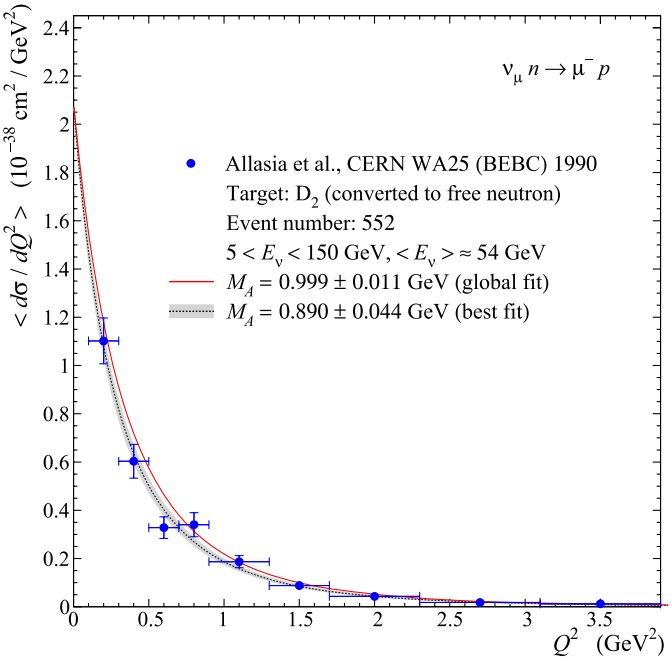

Fig. 5. Flux-weighted differential cross section for $\nu_\mu n \to \mu^- p$ measured in the WA25 experiment with the CERN bubble chamber BEBC filled with deuterium and exposed to high-energy ν_μ beam at the CERN-SPS [60]. The data were converted to a free neutron target by the authors of the experiment. The curves are the calculated cross sections averaged over the experimental ν_μ energy spectrum borrowed from [120]. The energy range and estimated mean energy are given in the legend. The *dashed curves* are for the best fit to the WA25 data, while the *solid curves* correspond to the global fit to all QES data. *Shaded band* represents 1σ deviation from the best-fitted value of $M_{\rm A}$ given in the legend

All the deuterium data quoted in Fig. 2 and freon data in Fig. 3 were converted to a free nucleon target by the experimenters.[4] The BNL 1981 experiment [25] had reported the E_ν and Q^2 dependencies of $M_{\rm A}$ extracted from a fit of the experimental Q^2 distribution rather than the cross section; we quote the BNL 1981 cross section recalculated from $M_{\rm A}$ by Kitagaki et al. [35]. Similarly, the FNAL 1984 rectangle [36, 37] and FNAL 1987 datapoint [39] were calculated by the experimenters (for free proton target) using the $M_{\rm A}$ value extracted from the measured Q^2 distribution of $\overline{\nu}_\mu$ events recorded in the Fermilab 15' bubble chamber filled with a heavy neon–hydrogen mixture. The data from several freon experiments (e.g., [43, 48, 104]) reported in the original papers in units cm^2 per nucleon of freon nucleus, were converted to the standard units.

All solid curves shown in the figures were calculated using the BBBA(07) model for vector form factors with $d/u = 0$ and always correspond to the best fit value

$$M_{\rm A}^{\nu+\overline{\nu}} = 0.999 \pm 0.011\,{\rm GeV} \quad (\chi^2/{\rm NDF} \approx 1.3)\,, \quad (12)$$

obtained from the global fit of neutrino and antineutrino data on the total and differential cross sections (see Table 2). We do not show the cross sections calculated with the GKex(05) model since the difference will be practically invisible.

[4] The nuclear corrections applied to the deuterium data under consideration, were treated according to Singh [121]. The nuclear effects for the freon data were modeled using a Fermi gas approach.

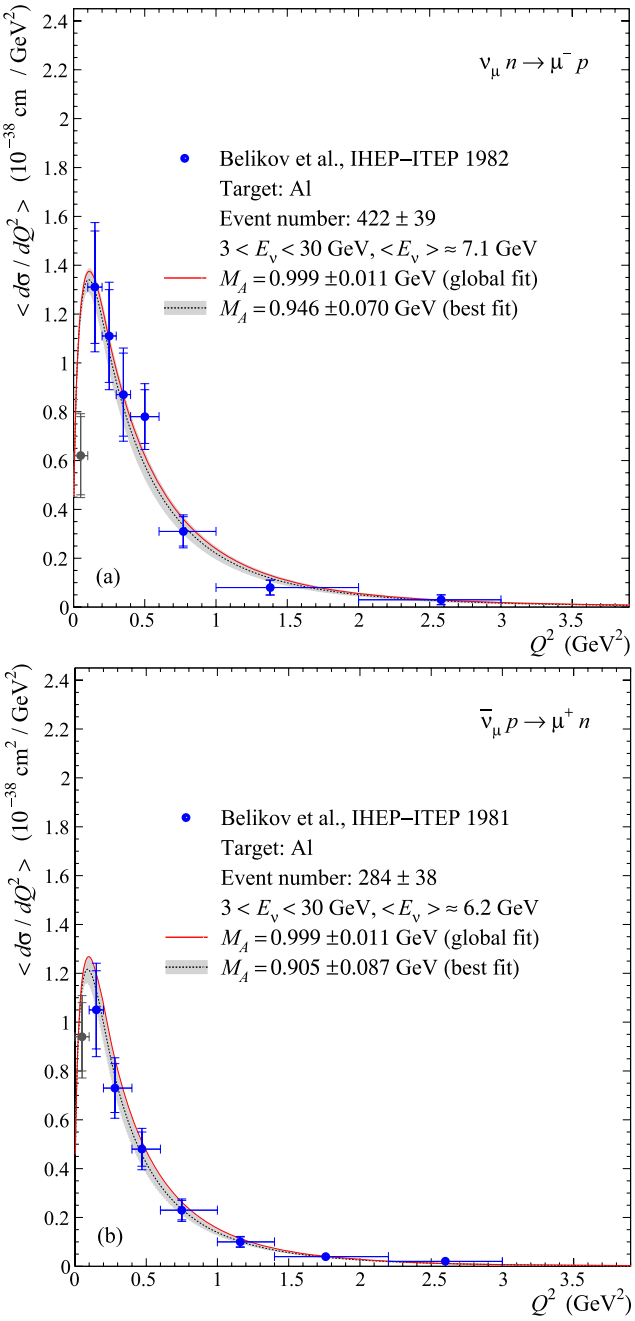

Fig. 6. Flux-weighted differential cross sections for $\nu_\mu n \to \mu^- p$ (**a**) and $\overline{\nu}_\mu p \to \mu^+ n$ (**b**) measured in the IHEP-ITEP experiment with a spark chamber detector with aluminium filters and exposed to the U70 broad-band ν_μ and $\overline{\nu}_\mu$ beams of the Serpukhov PS [66, 68]. The *inner* and *outer bars* indicate statistical and total errors, respectively; the overall systematic error of about 10% is due mainly to uncertainties of the flux normalization and scanning/triggering efficiencies. The *curves* are the calculated cross sections averaged over the experimental ν_μ and $\overline{\nu}_\mu$ energy spectra borrowed from [71, 111]. The energy range and estimated mean energies are given in the legends. The *dashed curves* are for the best fit to the IHEP-ITEP data, while the *solid curves* correspond to the global fit to all QES data. The *points* shown by *grey symbols* are excluded from the fits (see text). *Shaded bands* represent 1σ deviations from the best-fitted values of M_A given in the legends

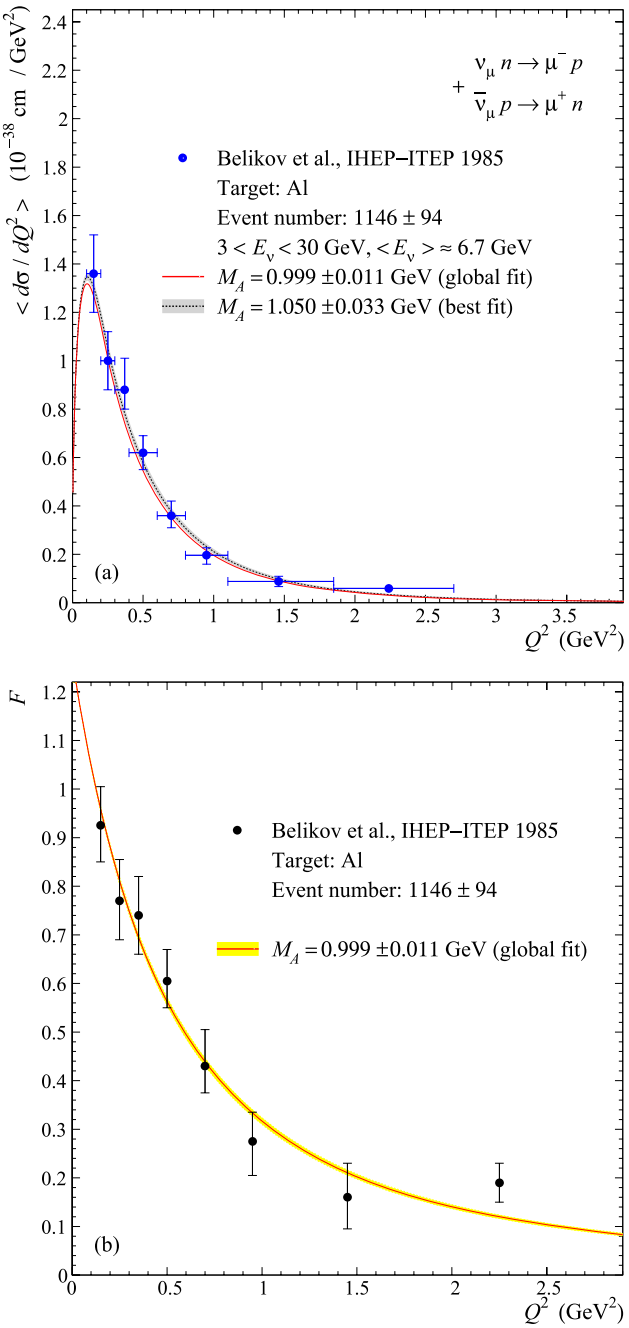

Fig. 7. Flux-weighted semisum of differential cross sections for $\nu_\mu n \to \mu^- p$ and $\overline{\nu}_\mu p \to \mu^+ n$ (**a**) and axial-vector form factor $F_\mathrm{A}(Q^2)$ (**b**) measured in the IHEP-ITEP experiment with a spark chamber detector with aluminium filters and exposed to the U70 broad-band ν_μ and $\overline{\nu}_\mu$ beams of the Serpukhov PS [71]. The error bars represent the total errors which include the overall systematic error of about 10% (due mainly to uncertainties of the flux normalization and scanning/triggering efficiencies). The *curves* in panel (**a**) are the calculated semisum of the cross sections each averaged over the experimental ν_μ and $\overline{\nu}_\mu$ energy spectra borrowed from [71, 111]. The energy range and estimated mean energy are given in the legend. The *dashed curve* is for the best fit to the quoted IHEP-ITEP data, while the *solid curve* corresponds to the global fit to all QES data. *Shaded bands* in panels (**a**) and (**b**) represent 1σ deviations from the best-fitted values of M_A given in the legends

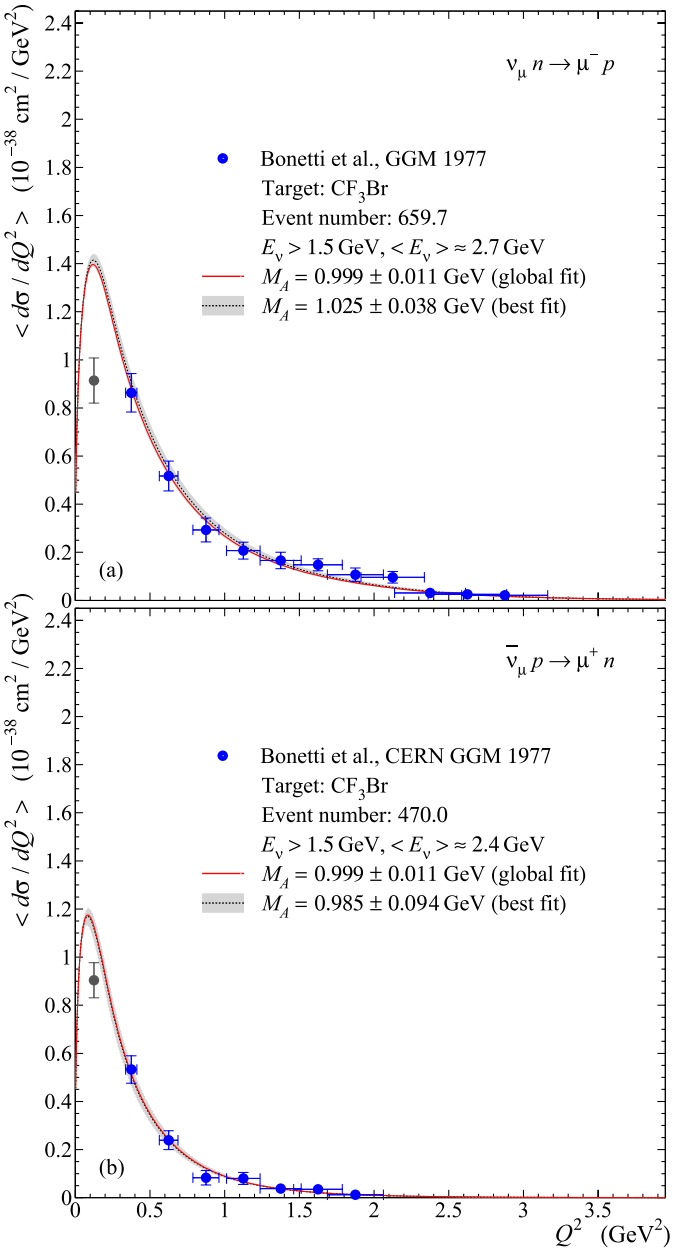

Fig. 8. Flux-weighted differential cross sections for $\nu_\mu n \to \mu^- p$ (**a**) and $\overline{\nu}_\mu p \to \mu^+ n$ (**b**) measured with the heavy-liquid bubble chamber Gargamelle filled with heavy freon and exposed to the CERN-PS ν_μ and $\overline{\nu}_\mu$ beams [53, 108]. The *error bars* contain the statistical fluctuation and the indetermination on the ν_μ and $\overline{\nu}_\mu$ fluxes. The *curves* are the calculated cross sections averaged over the experimental ν_μ and $\overline{\nu}_\mu$ energy spectra given in [53]. Only the events with $E_{\nu,\overline{\nu}} > 1.5$ GeV were accepted. The *dashed curves* are for the best fit to the GGM 1977 data, while the *solid curves* correspond to the global fit to all QES data. The *points* shown by *grey symbols* are excluded from the fits (see text). *Shaded bands* represent 1σ deviations from the best-fitted values of M_A given in the legends

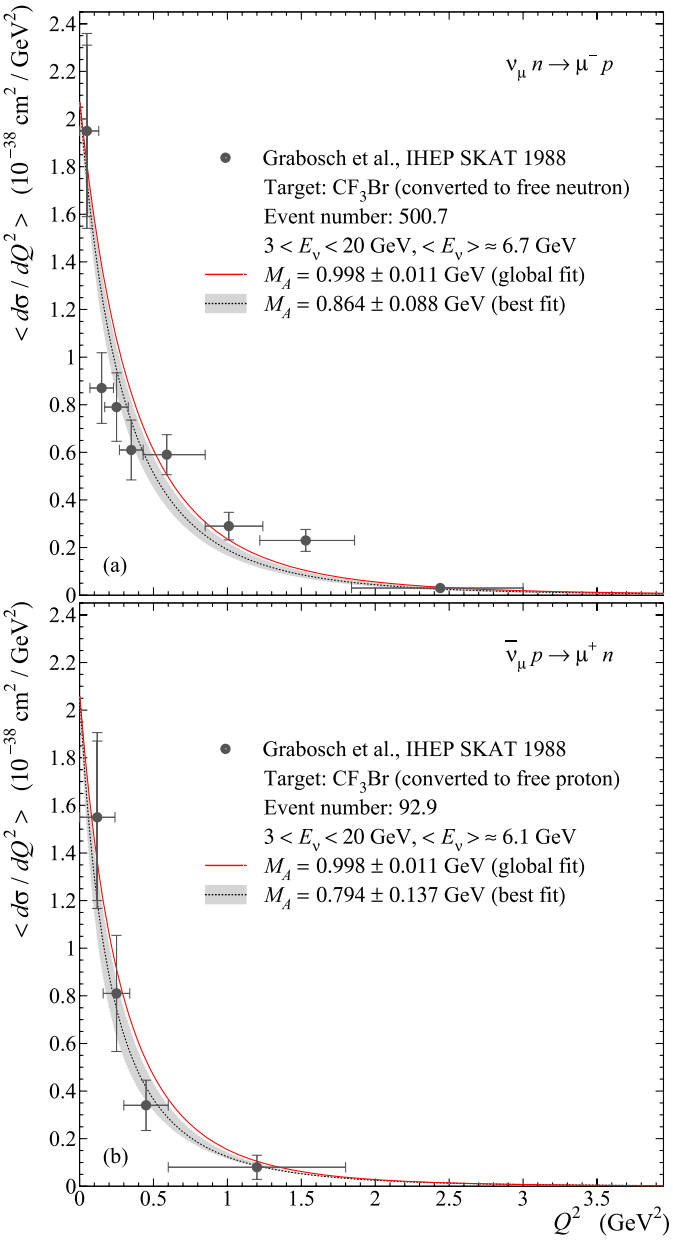

Fig. 9. Flux-weighted differential cross sections for $\nu_\mu n \to \mu^- p$ (**a**) and $\overline{\nu}_\mu p \to \mu^+ n$ (**b**) measured with the freon filled bubble chamber SKAT exposed to the U70 broad-band ν_μ and $\overline{\nu}_\mu$ beams of the Serpukhov PS [73, 111] (see also [72] for the earlier analyses of the same data sample). The data were converted to a free nucleon target by the authors of the experiment. The *inner* and *outer bars* indicate statistical and total errors, respectively; the systematic error includes the uncertainties due to the cross section normalization and nuclear Monte Carlo. The *curves* are the calculated cross sections averaged over the experimental ν_μ and $\overline{\nu}_\mu$ energy spectra borrowed from [111]. The energy range and estimated mean energies are given in the legends. The *dashed curves* are for the best fit to the SKAT 1988 data, while the *solid curves* correspond to the global fit to all QES data (the SKAT 1988 data are excluded from the global fit). *Shaded bands* represent 1σ deviations from the best-fitted values of M_A given in the legends

The dashed curves in Fig. 2 are calculated with the M_A values extracted from the best fit to the (preliminary) NOMAD total cross section data

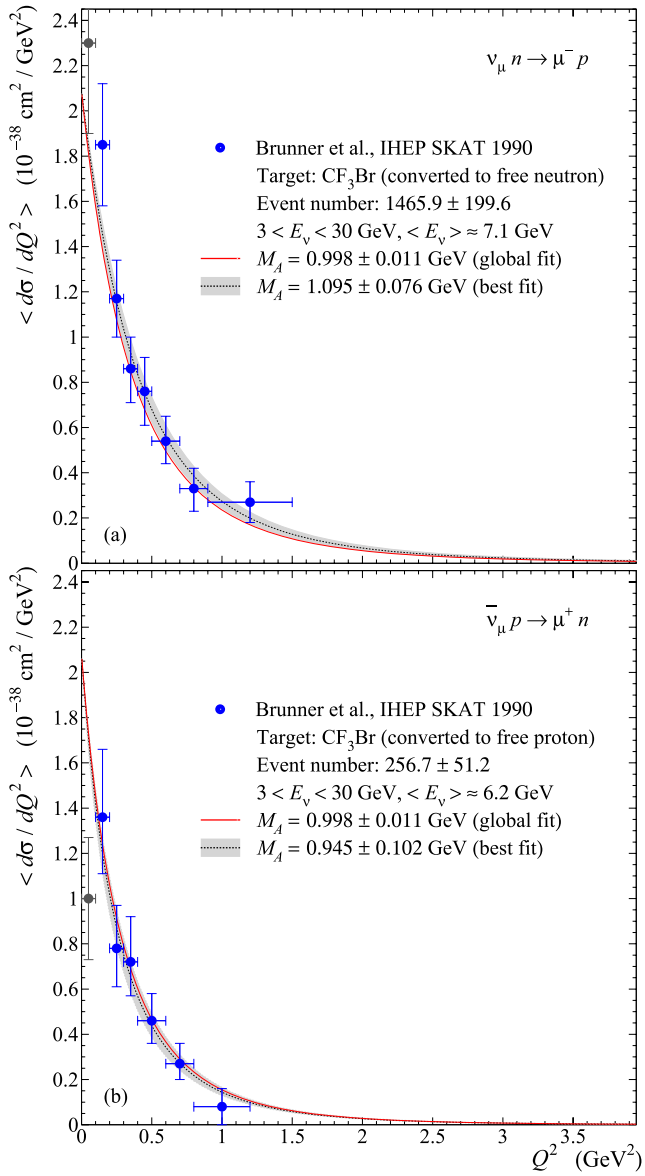

Fig. 10. Flux-weighted differential cross sections for $\nu_\mu n \to \mu^- p$ (**a**) and $\overline{\nu}_\mu p \to \mu^+ n$ (**b**) measured with the freon filled bubble chamber SKAT exposed to the U70 broad-band ν_μ and $\overline{\nu}_\mu$ beams of the Serpukhov PS [74]. The data were converted to a free nucleon target by the authors of the experiment. The *inner* and *outer bars* indicate statistical and total errors, respectively; the systematic error includes the uncertainties due to the cross section normalization and nuclear Monte Carlo. The *curves* are the calculated cross sections averaged over the experimental ν_μ and $\overline{\nu}_\mu$ energy spectra borrowed from [111]. The energy range and estimated mean energies are given in the legends. The *dashed curves* are for the best fit to the SKAT 1990 data, while the *solid curves* correspond to the global fit to all QES data. The *points* shown by *grey symbols* are excluded from the fits (see text). *Shaded bands* represent 1σ deviations from the best-fitted values of M_A given in the legends

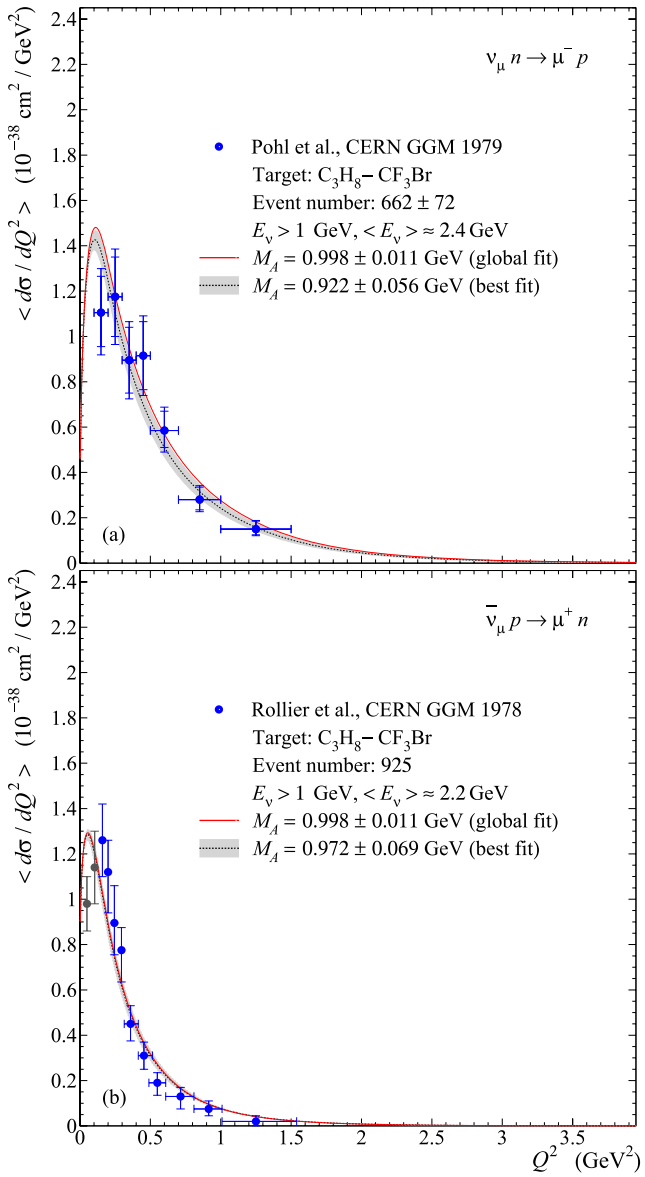

Fig. 11. Flux-weighted differential cross sections for $\nu_\mu n \to \mu^- p$ (**a**) and $\overline{\nu}_\mu p \to \mu^+ n$ (**b**) measured with the bubble chamber Gargamelle filled with light propane-freon mixture and exposed to the CERN-PS ν_μ and $\overline{\nu}_\mu$ beams [55, 58]. The *inner* and *outer bars* in panel (**a**) indicate statistical and total errors, respectively; the error bars in panel (**b**) contain the statistical fluctuation and the indetermination on the $\overline{\nu}_\mu$ flux. The *curves* are the calculated cross sections averaged over the experimental ν_μ and $\overline{\nu}_\mu$ energy spectra given in [53] and [59], respectively. Only the events with $E_{\nu,\overline{\nu}} > 1$ GeV were accepted. The *dashed curves* are for the best fit to the GGM data, while the *solid curves* correspond to the global fit to all QES data. The *points* shown by *grey symbols* are excluded from the fits (see text). *Shaded bands* represent 1σ deviations from the best-fitted values of M_A given in the legends

alone [64]:

$$M_A^\nu = 1.05 \pm 0.02_{\rm stat} \pm 0.07_{\rm syst}\ {\rm GeV}\,,$$

$$M_A^{\overline{\nu}} = 1.06 \pm 0.07_{\rm stat} \pm 0.12_{\rm syst}\ {\rm GeV}\,, \qquad (13)$$

both agree with the global fit value (12). Note that these results were obtained with the GKex(05) vector form fac-

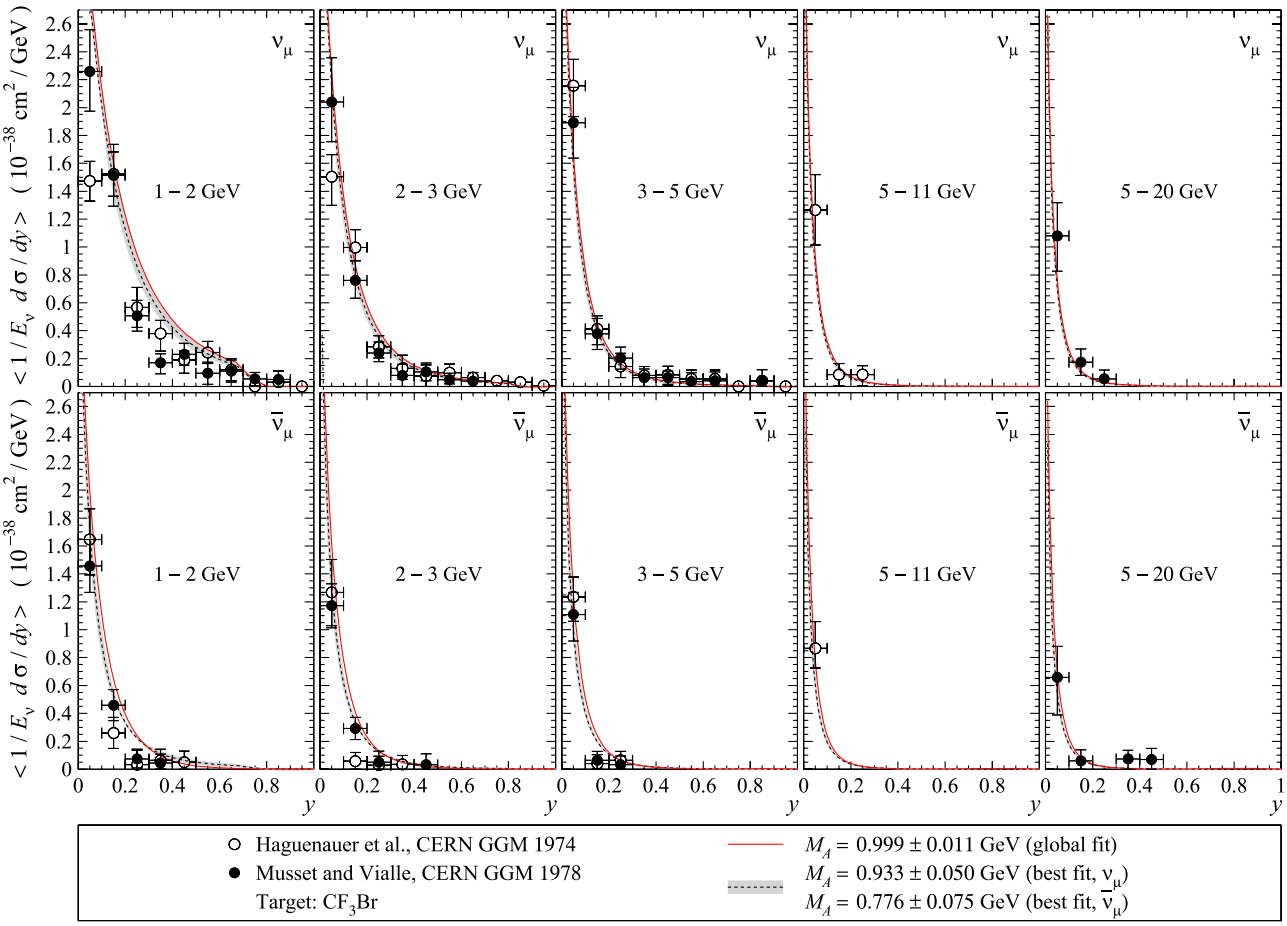

Fig. 12. Flux-weighted differential cross sections $(1/E_\nu)\,\mathrm{d}\sigma(\nu_\mu n \to \mu^- p)/\mathrm{d}$ (*top panels*) and $(1/E_\nu)\,\mathrm{d}\sigma(\overline{\nu}_\mu p \to \mu^+ n)/\mathrm{d}y$ (*bottom panels*) measured with the heavy freon filled bubble chamber Gargamelle exposed to the wide-band CERN-PS ν_μ and $\overline{\nu}_\mu$ beams [50, 108]. The data from [50] (range 5–11 GeV) and [108] (ranges 1–2, 2–3, 3–5, and 5–20 GeV) represent two different analyses of the same data sample (see also [49, 52, 112] for other versions). The measured cross sections were converted to a free nucleon target by the authors of the experiment. The quoted error bars are the total errors which include the uncertainties in the ν_μ and $\overline{\nu}_\mu$ fluxes and nuclear Monte Carlo. The *curves* are for the calculated cross sections averaged (for each energy range indicated in the panels) over the experimental ν_μ and $\overline{\nu}_\mu$ energy spectra taken from [108]. The *dashed curves* correspond to the M_A values obtained by fitting the GGM 1978 data from the energy ranges 2–3, 3–5, and 5–20 GeV and GGM 1974 data from the range 5–11 GeV (separately for neutrino and antineutrino cross sections). The range 1–2 GeV is excluded from the analysis in order to minimize the error in modelling the nuclear effects. The *solid curves* correspond to the global fit to all QES data (the GGM data are not included in this fit). *Shaded bands* represent 1σ deviations from the best-fitted values of M_A given in the legend

tors. Fitting the NOMAD data with the BBBA(07) form factors increases M_A^ν and $M_\mathrm{A}^{\overline{\nu}}$ by about 0.8 and 0.9%, respectively, that still remains well within the errors quoted in (13).

As is seen from the figures, the obtained result, despite the non-optimal χ^2 and large spread of the data, is not in conflict with the main part of the data excluded from the global fit. Moreover, it well agrees with the world averaged value of

$$M_\mathrm{A} = 1.014 \pm 0.014\,\mathrm{GeV}\,, \qquad (14)$$

obtained in [3] as a result of their reanalysis of the "raw" data from $\nu_\mu d$ and $\overline{\nu}_\mu H$ experiments ANL 1973 [15], ANL 1977 [18], ANL 1982 [19], BNL 1980 [24], BNL 1981 [25], BNL 1983 [122], BNL 1990 [31], FNAL 1983 [35], CERN BEBC 1990 [60], and from pion electroproduction experiments after corrections for hadronic effects. Note that the values of M_A re-extracted in [3] from each $\nu_\mu d$ experiment separately spread between 0.97 ± 0.05 and 1.04 ± 0.06 GeV. It exceeds the difference between the results of our analysis of data on total and differential cross sections. Both analyses use the same BBBA(07) model and mutually supplement each other, since they practically do not overlap in the adopted data sets. Formal averaging of the values (12) and (14) yields

$$M_\mathrm{A} = 1.006 \pm 0.009\,\mathrm{GeV}\,.$$

4.3 Are $M_{\rm A}^{\nu}$ and $M_{\rm A}^{\overline{\nu}}$ really different?

According to the global fit (see Table 2), the difference between the values of $M_{\rm A}^{\nu}$ and $M_{\rm A}^{\overline{\nu}}$ obtained by fitting the neutrino and antineutrino data separately, reaches about 3.5% for BBBA(07) and about 3.2% for GKex(05) that is above the statistical error in determination of $M_{\rm A}^{\nu}$ and $M_{\rm A}^{\overline{\nu}}$. However, taking into account the systematic difference between the fits of total and differential cross section data, as well as high values of χ^2/NDF, this difference cannot be considered statistically significant. Furthermore, the fit to the antineutrino data is not stable relative to including/excluding some data subsets. In particular, as is seen from Fig. 2, the total NuTeV cross sections per nucleon bound in iron, averaged over the energy range $E_{\nu,\overline{\nu}} = 30$–$300\,\mathrm{GeV}$

$$\overline{\sigma}(\nu_\mu n \to \mu^- p) = (0.94 \pm 0.03_{\rm stat} \pm 0.07_{\rm syst}) \times 10^{-38}\,\mathrm{cm}^2,$$
$$\overline{\sigma}(\overline{\nu}_\mu p \to \mu^+ n) = (1.12 \pm 0.04_{\rm stat} \pm 0.10_{\rm syst}) \times 10^{-38}\,\mathrm{cm}^2$$

(shown in Fig. 2 by rectangles) notably exceed the corresponding best fit curves whereby the NuTeV data [40] strongly affects the global fit values of $M_{\rm A}^{\nu}$ and $M_{\rm A}^{\overline{\nu}}$.

To clarify this point further, we have performed additional fits, in which the datasets obtained in experiments with non-active targets have been removed. Namely, we excluded the highest energy NuTeV total cross section data (iron target) [40] and the data on differential cross sections measured with the IHEP-ITEP spark chamber detector with aluminium filters [66, 68, 71], since these experiments do not have an active target to measure recoil hadrons and surely remove resonance background. In order to minimize possible uncertainties in nuclear corrections, the lowest-energy CERN 1967 total cross section data (freon target) [43] were also excluded from these fits. The results of this analysis are summarized in Table 3. It is seen that the additional reduction of the dataset essentially *decreases* the resulting values of $M_{\rm A}$. Concurrently it improves the statistical quality of the fits to the total cross section data, while slightly increases the χ^2/NDF for the fit to the differential cross sections. Besides that, the $M_{\rm A}$ values extracted from the total and differential cross sections become bit more consistent. The differences between $M_{\rm A}^{\nu}$ and $M_{\rm A}^{\overline{\nu}}$ [$-65\,\mathrm{MeV}$ for BBBA(07) and $-75\,\mathrm{MeV}$ for GKex(05)] become *opposite in sign* to those obtained from our "default" fit performed with the full dataset. However, both $M_{\rm A}^{\nu}$ and $M_{\rm A}^{\overline{\nu}}$ values are still compatible, within the 1σ deviation, with the average value of $M_{\rm A}^{\nu+\overline{\nu}}$. So we may reckon that

(i) the axial mass extraction is rather responsive to the choice of the data subsets and
(ii) the current experimental data cannot definitely confirm or disconfirm possible difference between the axial masses extracted from experiments with neutrino and antineutrino beams.

Similar fit performed for the differential cross section data only, from which all the $\nu_\mu d$ data were excluded, leads to an *increase* of $M_{\rm A}^{\nu}$ by about 4.2% (4.4%) for BBBA(07) (GKex(05)). However, the statistical error of this fit increases too. Including into this fit the non-deuterium data on total cross sections diminish the increase of $M_{\rm A}^{\nu}$ to about 1.2% for both BBBA(07) and GKex(05). Hence, the above conclusions remain essentially unchanged.

4.4 Further details on differential cross section data

As is known from the comparison with the low-energy electron-nucleus scattering data, the RFG description of the low-Q^2 region is not enough accurate especially at energies below $\sim 2\,\mathrm{GeV}$ (for recent discussion, see, e.g., [123, 124] and references therein). Moreover, the shape of $\mathrm{d}\sigma/\mathrm{d}Q^2$ at $Q^2 \lesssim 0.1\,\mathrm{GeV}^2$ is slowly sensitive to variations of $M_{\rm A}$ (see below). Thus, in order to minimize possible uncertainties due to nuclear effects, the points with $Q^2 < 0.15\,\mathrm{GeV}^2$ were rejected from the fit of the differential cross section dataset. Leaving these points in the fit would lead to a *decrease* of the output values of $M_{\rm A}^{\nu}$, $M_{\rm A}^{\overline{\nu}}$, and $M_{\rm A}^{\nu,\overline{\nu}}$ obtained from the $\mathrm{d}\sigma/\mathrm{d}Q^2$ dataset by, respectively, 1.8, 3.3, and 2.2% for BBBA(07) and 2.0, 4.0, and 2.6% for GKex(05) form factors. The corresponding decrease of $M_{\rm A}$ derived from the full dataset (σ and $\mathrm{d}\sigma/\mathrm{d}Q^2$) is clearly less essential: respectively, 0.7, 1.3, and 0.9% for BBBA(07) and 0.7, 1.5, and 1.0% for GKex(05).

Of course, the mentioned uncertainty still remains in the RFG calculations of the total cross sections, since the contribution from the low-Q^2 region is essential at low energies. To illustrate this, we show in Fig. 4 the relative contribution of the region $Q^2 < Q_1^2$ into the total cross section, $R\left(Q_1^2\right) = \sigma\left(Q^2 < Q_1^2\right)/\sigma$, as a function of Q_1^2, evaluated for ν_μ and $\overline{\nu}_\nu$ QE interactions with carbon at several (anti)neutrino energies using $M_{\rm A} = 1\,\mathrm{GeV}$.[5] It is seen that for neutrino-nucleus interactions $R \lesssim 0.25$ as $Q_1^2 < 0.15\,\mathrm{GeV}^2$ and $E_\nu > 0.7\,\mathrm{GeV}$ that is for all energies of our current interest. As a result, a few percent error expected in $\mathrm{d}\sigma/\mathrm{d}Q^2$ due to inaccuracy of the RFG model for the low-Q^2 region, becomes nearly negligible in the total cross section. However it is not the case for antineutrino interactions, for which the ratio $R\left(Q_1^2 = 0.15\,\mathrm{GeV}^2\right)$ becomes reasonably small ($R \lesssim 0.3$) only for $E_\nu \gtrsim 2\,\mathrm{GeV}$. Therefore the lower energy antineutrino total cross section data may bias an uncontrolled (while still small) additional uncertainty. Fortunately, the major part of the data participated in the global fit satisfies the above conditions and our examination demonstrates that the related uncertainty is not weighty.

Figures 5–7a and 8–11 represent the spectrum-averaged differential cross sections for several nuclear targets: deuterium (Fig. 5) [60], aluminium (Figs. 6 and 7a) [66, 68, 71], freon (Figs. 8–10) [53, 73, 74, 108, 111], and propane–freon mixture (Fig. 11) [55, 58]. In Fig. 7b we show (for illustrative purposes only) the axial-vector form factor extracted in the IHEP-ITEP spark chamber experiment [71]. All the quoted data, except those from [73] (superseded by the data from the more recent publica-

[5] Here $\sigma\left(Q^2 < Q_1^2\right)$ is defined as an integral of $\mathrm{d}\sigma/\mathrm{d}Q^2$ from the kinematical minimum of Q^2 to $Q^2 = Q_1^2$.

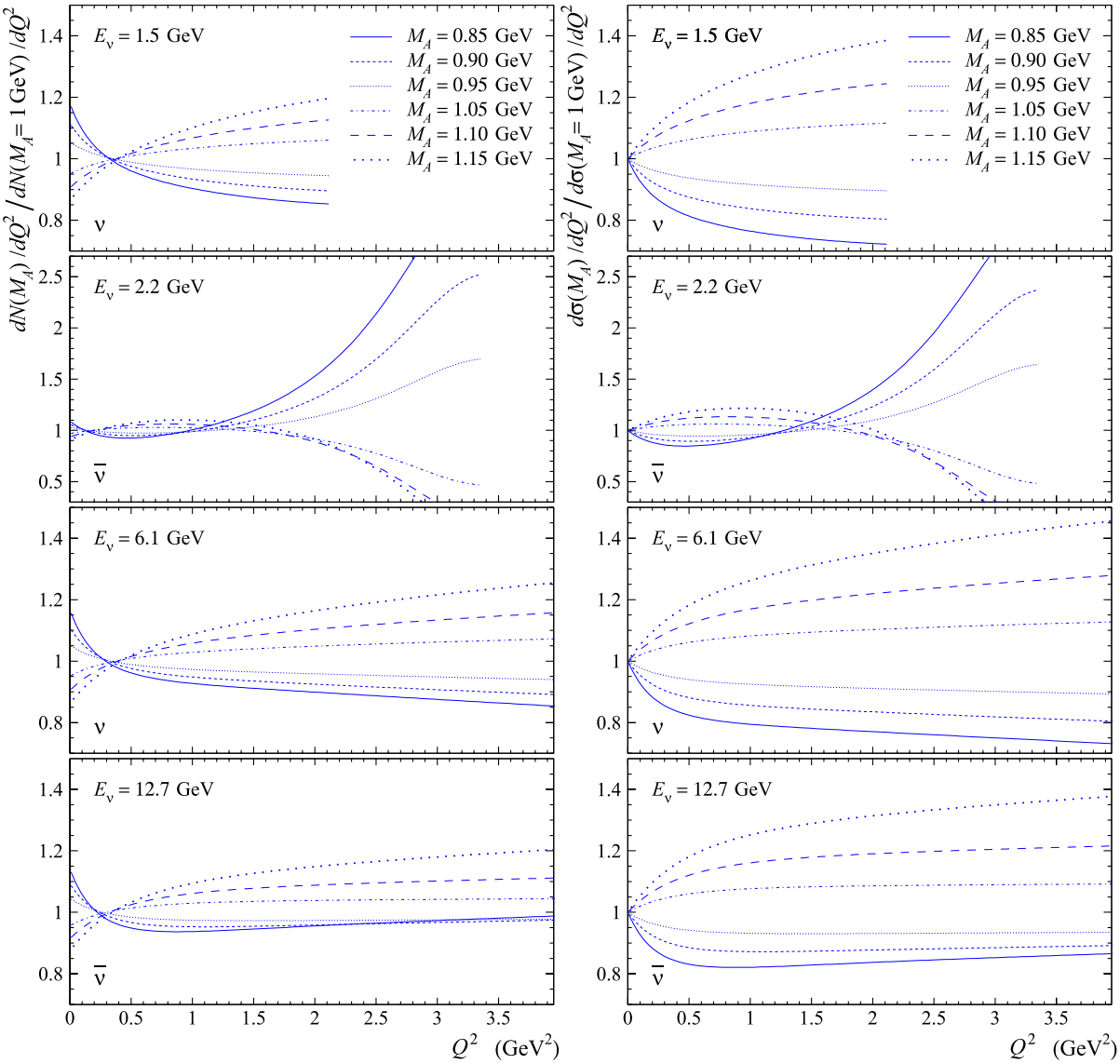

Fig. 13. The distributions $\mathrm{d}N/\mathrm{d}Q^2$ and differential cross sections $\mathrm{d}\sigma/\mathrm{d}Q^2$ vs. Q^2 for $\nu_\mu n$ and $\overline{\nu}_\mu p$ quasielastic scattering, calculated with different $M_\mathrm{A} = 0.85$, 0.90, 0.95, 1.05, 1.10, and 1.15 GeV and normalized to the corresponding quantities calculated with $M_\mathrm{A} = 1$ GeV at four fixed values of energy corresponding to the mean (anti)neutrino beam energies in experiments HLBC 1969 [46], Gargamelle 1979 [59], SKAT 1981 [65], and FNAL 1984 [36, 37] (see Figs. 14–17 below). The *curves* in the four *upper panels* end up at the kinematical boundaries

tion by the SKAT Collaboration [74]), model-dependent IHEP-ITEP data on $F_\mathrm{A}(Q^2)$ [71], and a few rejected low-Q^2 datapoints, participate in the global fit. We show the cross sections calculated with M_A obtained by individual fits to the data of each experiment alone and compare these against the cross sections evaluated with the global-fit value of M_A. All the details are recounted in the captions and legends of the figures. The comparison demonstrates that the individual and global fits generally do not contradict each other. The differences are within the experimental errors and are not of systematic nature.

As a further test of the global fit, we show in Fig. 12 the flux-weighted differential cross sections $\mathrm{d}\sigma(\nu_\mu n \to \mu^- p)/\mathrm{d}y$ and $\mathrm{d}\sigma(\overline{\nu}_\mu p \to \mu^+ n)/\mathrm{d}y$ (divided by energy), which were measured with the Gargamelle bubble chamber filled with liquid freon and exposed to the wide-band CERN-PS ν_μ and $\overline{\nu}_\mu$ beams. Several analyses of these data samples are available from the literature (see [49, 50, 52, 108] and also [112] for a review). Figure 12 shows two representative versions taken from [50, 108] – the preliminary and final results of the GGM experiment, respectively. The data are shown for the five narrow instrumental ranges: 1–2, 2–3, 3–5, 5–11, and 5–20 GeV. The measured cross sections were converted freon to a free nucleon target by the experimenters, after accounting for Fermi motion of the nucleons and Pauli suppression of quasielastic events.

For a qualitative comparison, we have performed individual fits to the GGM data, separately for neutrino and antineutrino differential cross sections. In order to reduce possible error introduced by RFG calculations of nuclear effects, the energy range of 1–2 GeV has been excluded from this likelihood analysis. As is seen from the figure, the M_A value extracted from the neutrino subsample does not contradict to that from the global fit, while it is not so for the antineutrino data subsample where the discrepancy is essential. This discrepancy can be attributed (at least, partially) to the vagueness of the model for nuclear effects used in the analyses of the GGM data. Since the details of the GGM nuclear Monte Carlo are not available, we do not include this data sample into the global fit. We note, however, that the inclusion of these data (also without the low-energy datapoints) into the fit only leads to a small *decrease* of the output values of M_A^{ν}, $M_A^{\overline{\nu}}$, and $M_A^{\nu,\overline{\nu}}$ – by, respectively, 0.4, 2.2, and 0.9% for BBBA(07) and 0.3, 2.0, and 0.8% for GKex(05) form factors. The corresponding χ^2/NDF values remain nearly the same.

4.5 Q^2 distributions

An additional fruitful set of available data is the Q^2 distributions dN/dQ^2 of the QES events measured in several experiments with different nuclear targets. Usually just dN/dQ^2 is considered as the observable most appropriate for extracting axial mass value, since it is less dependent of the flux and spectrum uncertainties in comparison with the differential or total cross sections. However, in comparison with the differential cross section, the Q^2 distribution has two drawbacks: it contains an uncertainty due to normalization, and it is generally less responsive to variations of M_A at high Q^2. Figure 13 illustrates the second point. It shows the Q^2 distributions and differential cross sections for ν_μ and $\overline{\nu}_\mu$ quasielastic scattering off free nucleons, evaluated with different values of M_A and normalized to the corresponding quantities calculated with $M_A = 1$ GeV. The calculations are done with the fixed values of energy corresponding to the mean (anti)neutrino beam energies in experiments [37, 46, 59, 65]. It is seen from the figure that the region $Q^2 \lesssim 0.15\,\mathrm{GeV}^2$ strongly affected by the nuclear effects, is sensitive to M_A for dN/dQ^2 and less sensitive for $d\sigma/dQ^2$; the situation is opposite for the high Q^2 region for which the nuclear corrections are less important.

We use the measured Q^2 distributions for a consistency test of our analysis. For illustration, we show the four

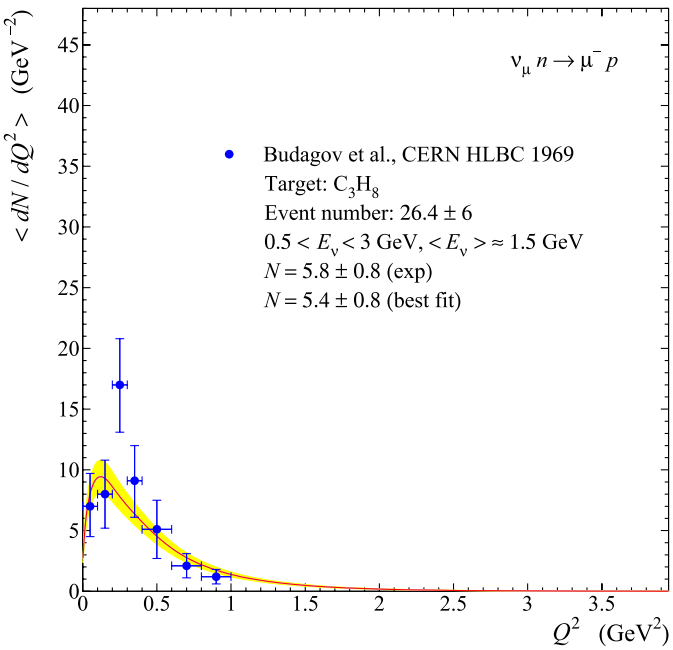

Fig. 14. Flux-weighted Q^2 distribution for $\nu_\mu n \to \mu^- p$ measured with the CERN heavy-liquid bubble chamber (HLBC) filled with propane and exposed to the CERN PS ν_μ beam [46]. The *curve* is the distribution calculated with M_A obtained from the global fit, averaged over the experimental ν_μ energy spectrum from [119], and normalized to the HLBC 1969 data. The spectrum is estimated to be accurate within ±15% (the error includes an estimate of systematic effects). The energy range and estimated mean energy are given in the legends. *Shaded band* represents 1σ variation from the average due to uncertainties in M_A and normalization factor N

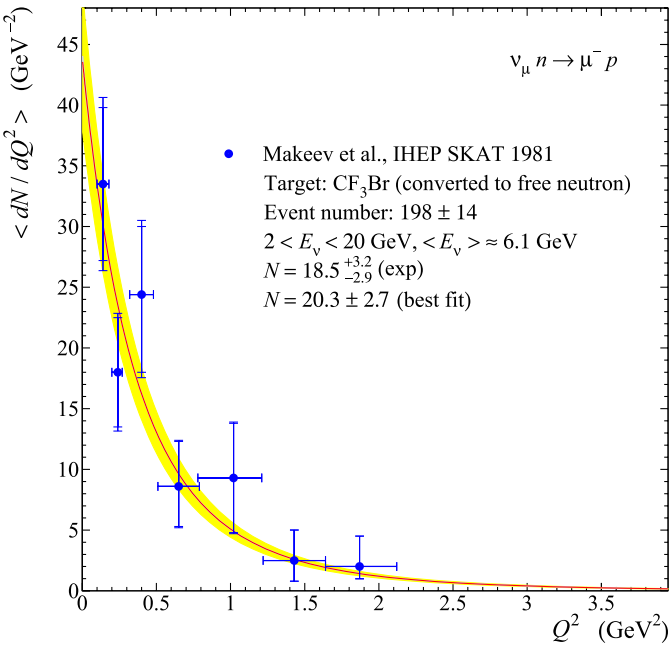

Fig. 15. Flux-weighted Q^2 distribution for $\nu_\mu n \to \mu^- p$ measured with the freon filled bubble chamber SKAT exposed to the U70 broad-band ν_μ beam of the Serpukhov PS [65]. The data were converted to a free nucleon target by the authors of the experiment. The *inner* and *outer bars* indicate statistical and total errors, respectively; the systematic error includes the uncertainties due to the flux normalization and nuclear Monte Carlo. The *curve* is the distribution calculated with M_A obtained from the global fit, averaged over the experimental ν_μ energy spectrum from [111], and normalized to the SKAT 1981 data. The energy range and estimated mean energy are given in the legends. *Shaded band* represents 1σ variation from the average due to uncertainties in M_A and normalization factor N

sets of data on Q^2 distributions measured in experiments HLBC 1969 (propane) [46] (Fig. 14), IHEP SKAT 1981 (freon) [65] (Fig. 15), CERN GGM 1979 (propane–freon mixture) [59] (Fig. 16), and FNAL E180 (neon–hydrogen mixture) [36, 37] (Fig. 17). The curves shown in the figures are calculated with the global-fit M_A and normalized to the data after fitting of the normalization factor N. The shaded bands indicate the uncertainty due mainly to indetermination of this factor. The obtained best-fit values of N should be compared with these evaluated directly from the experimental data (all values are shown in the legends of the figures). One can see that the agreement is excellent everywhere. So, we may conclude that this test was quite successful.

Another important confirmation of our result is a reasonably good agreement with the M_A value extracted in our earlier analysis of the data on total inelastic $\nu_\mu N$ and $\overline{\nu}_\mu N$ CC cross sections and relevant observables [125].

Finally, Fig. 18 presents a comparison of the total QES cross sections for ν_e, ν_μ, ν_τ, $\overline{\nu}_e$, $\overline{\nu}_\mu$, and $\overline{\nu}_\tau$ interactions with free nucleons, calculated with the obtained best-fit value of $M_A = 0.999 \pm 0.011$ GeV by using the BBBA(07) model of vector form factors. The shaded bands reproduce the uncertainty due to the 1σ error in M_A.

5 Discussion and conclusions

We performed a statistical study of the QES total and differential cross section data in order to extract the best-fit values of the parameters M_A. Our main results are summarized in Table 2 are, of course, model dependent and can be recommended for use only within the same (or numerically equivalent) model assumptions as in the present analysis. The best-fit values of the axial mass obtained by different fits do not contradict to each other and agree with the recent re-extraction of M_A from $\nu_\mu d$, $\overline{\nu}_\mu$H, and pion electroproduction experiments, reported in [3]. They are also in agreement with the *preliminary* result of high-statistical NOMAD experiment at CERN, as well as with the numerous earlier data which were not included into the likelihood analysis. It has been demonstrated that removing the data subsets obtained in experiments with non-active targets, particularly the NuTeV dataset, leads to a further *decrease* of the extracted values of M_A (see Table 3). In other words, there is no way to increase the M_A value which follows from essentially all (anti)neutrino data on total and differential QES cross sections.

On the other hand, our best-fit value of M_A is in a conflict with the mean values of M_A reported by K2K and

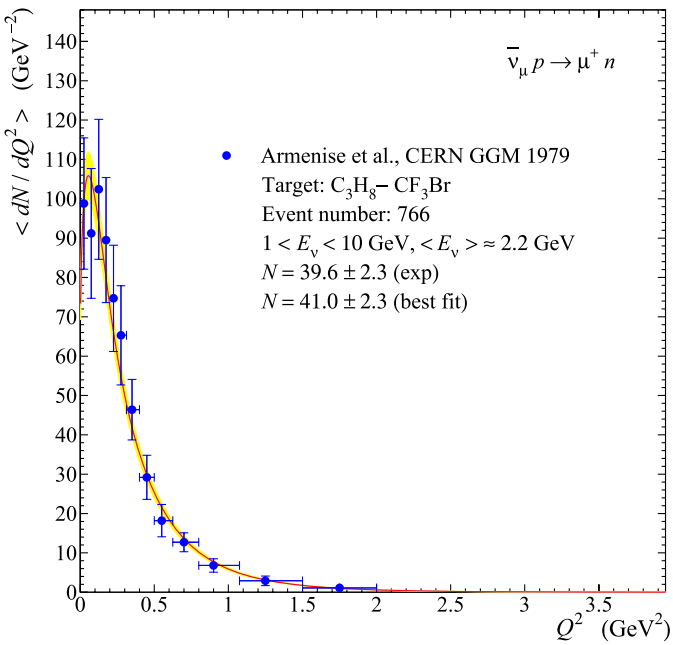

Fig. 16. Flux-weighted Q^2 distribution for $\overline{\nu}_\mu p \to \mu^+ n$ measured with the bubble chamber Gargamelle filled with light propane-freon mixture (87 mol. % of propane) and exposed to the CERN-PS $\overline{\nu}_\mu$ beam [59]. The *error bars* contain both statistical and systematic errors. The *curve* is the distribution calculated with M_A obtained from the global fit, averaged over the experimental $\overline{\nu}_\mu$ energy spectrum from [59], and normalized to the GGM 1979 data. The energy range and estimated mean energy are given in the legends. *Shaded band* represents 1σ variation from the average due to uncertainties in M_A and normalization factor N

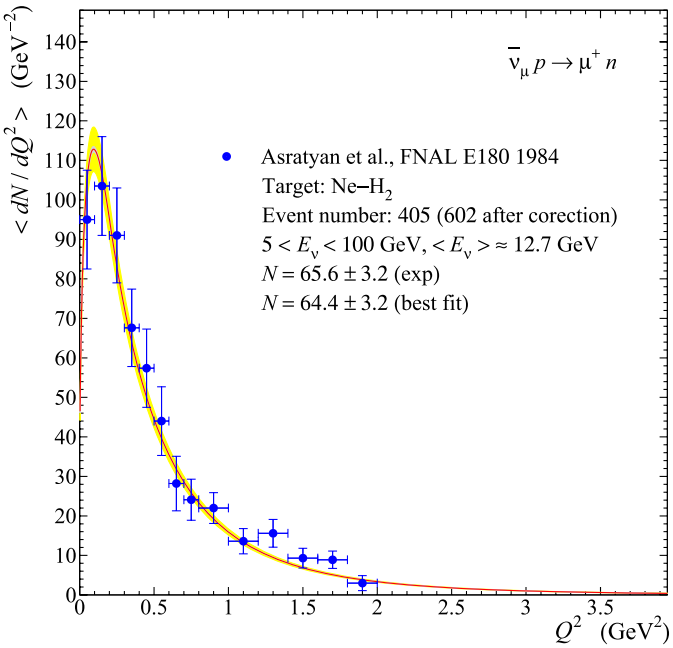

Fig. 17. Flux-weighted Q^2 distribution for $\overline{\nu}_\mu p \to \mu^+ n$ measured in the FNAL E180 experiment with a 15′ bubble chamber filled with heavy neon-hydrogen mixture (64% of neon atoms) and exposed to the FNAL wide-band $\overline{\nu}_\mu$ beam [36, 37] (see also [34] for an earlier version). The *curve* is the distribution calculated at the mean antineutrino energy of 12.7 ± 0.2 GeV, with M_A obtained from the global fit and then normalized to the E180 data. [The spectrum averaging procedure cannot be applied here, since the $\overline{\nu}_\mu$ spectrum has been evaluated just from the quoted Q^2 distribution.] *Shaded band* represents 1σ variation from the average due to uncertainties in M_A and normalization factor N

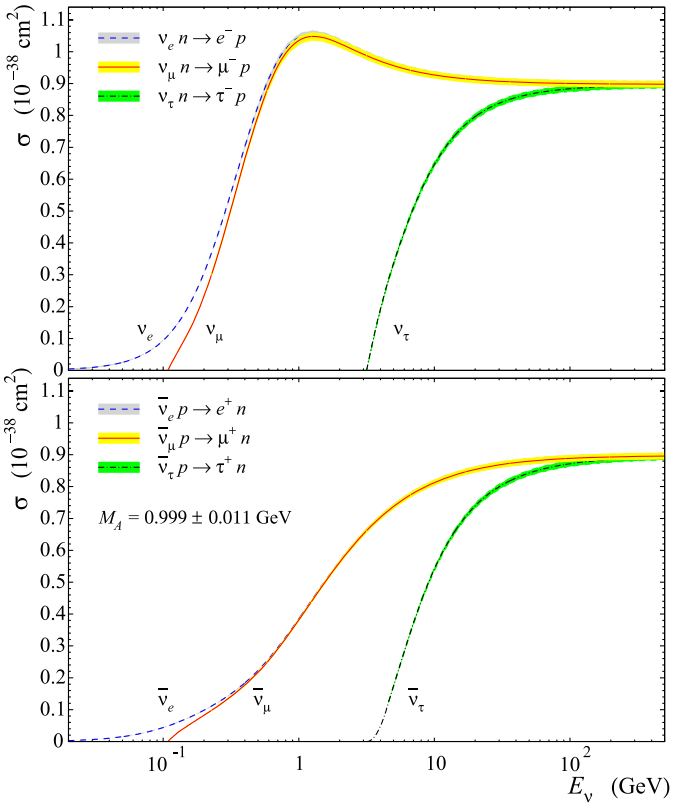

Fig. 18. Total quasielastic cross sections for electron, muon and τ neutrino and antineutrino interactions with free nucleons calculated with the best-fit value of $M_{\mathrm{A}} = 0.999 \pm 0.011$ GeV using the BBBA(07) vector form factors. *Shaded bands* represent the uncertainty due to the 1σ error in M_{A}

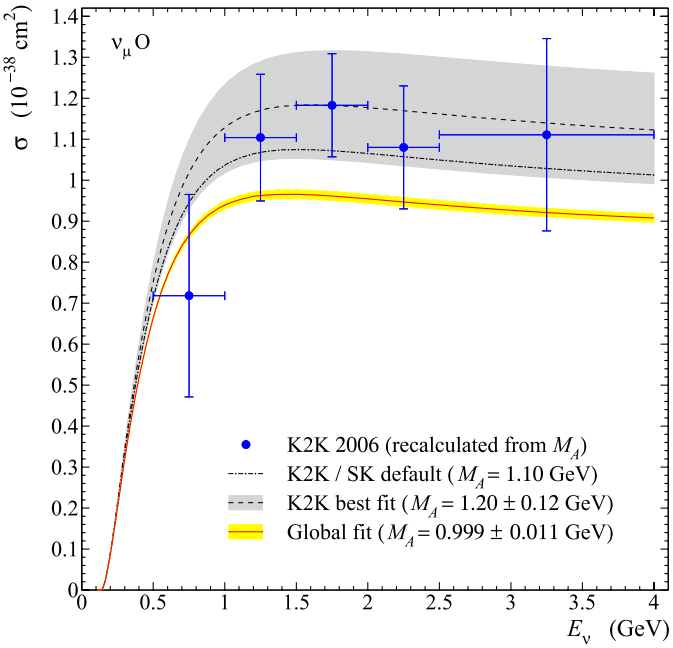

Fig. 19. Comparison between the QES ν_μ cross sections per neutron bound in oxygen, evaluated with several values of the axial mass. The *solid curve* with narrow band is calculated with our best fit value of M_{A}; the *dashed curve* with wide band corresponds to the K2K extraction of M_{A} [4]; the *dash-dotted curve* is calculated with the current K2K and Super-Kamiokande I default $M_{\mathrm{A}} = 1.1$ GeV [127, 128]. The *points* represent the K2K cross section reconstructed (with our version of RFG model and BBBA(07) vector form factors) from the best-fit values of M_{A} extracted for the five energy bins, as quoted in Fig. 9 of [4]

MiniBooNE Collaborations [4, 5], even after accounting for the maximum possible systematic error of our analysis related primarily to its susceptibility to the choice of the data subsets. To expound the problem, let us consider the representative K2K result with more details.

The M_{A} value reported in [4] has been obtained with a water target by fitting the Q^2 distributions of muon tracks reconstructed from neutrino-oxygen quasielastic interactions by using the combined K2K-I and K2K-IIa data from the Scintillating Fiber detector (SciFi) in the KEK accelerator to Kamioka muon neutrino beam. The experimental data from the continuation of the K2K-II period were not used in the analysis of [4]. The best-fit values of M_{A} obtained from the K2K-I and K2K-IIa data subsets separately are, respectively, 1.12 ± 0.12 GeV ($\chi^2/\mathrm{NDF} = 150/127$) and 1.25 ± 0.18 GeV ($\chi^2/\mathrm{NDF} = 109/101$).

Figure 19 shows the $\nu_\mu n \to \mu^- p$ total cross section per neutron bound in oxygen, recalculated from the fitted values of M_{A} derived in [4] from the Q^2 distribution shape for each reconstructed neutrino energy. It is necessary to underline here that the authors do not consider their result for each energy bin as a *measurement*, but rather a *consistency test*. All calculations represented in Fig. 19 were done with our default inputs that introduces an uncertainty of at most 2%; this uncertainty is added quadratically to the quoted error bars. Also shown are the cross sections evaluated by using our best fit value (12), the K2K value of 1.20 ± 0.12 GeV, and the value of 1.1 GeV used as a default in the recent neutrino oscillation analyses to the data from K2K [126, 127] and Super-Kamiokande I [128]. A significant systematic discrepancy is clearly seen at $E_\nu > 1$ GeV. Since the energy region covered by the K2K analysis extends to about 4 GeV, it seems problematic to explain this discrepancy by the inapplicability of the RFG model alone.

Considering that the low-energy K2K and MiniBooNE data are in agreement with each other and do not contradict to the high-energy NuTeV results, we may conclude that the new generation experiments for studying the quasielastic neutrino and antineutrino interactions with nucleons and nuclei are of urgent necessity, in order to resolve the inconsistencies between the old and new measurements of the axial-vector mass.

Acknowledgements. This study is currently supported by the Russian Foundation for Basic Research under Grant No. 07-02-00215-a. The authors would like to thank Krzysztof M. Graczyk, Sergey A. Kulagin, Dmitry V. Naumov, Jan T. Sobczyk, and Oleg V. Teryaev for helpful discussions. We thank the NOMAD Collaboration for permission to use their data prior to publication and Antonio Bueno for explaining us some points of LAr TPC experiment. We are especially grateful to

Arie Bodek for his constructive comments and suggestions. V.V.L. is very thankful to LPNHE (Paris) for warm hospitality and financial support during a stage of this work.

References

1. A. Liesenfeld et al., Phys. Lett. B **468**, 20 (1999) [arXiv: nucl-ex/9911003]
2. V. Bernard, L. Elouadrhiri, U.-G. Meißner, J. Phys. G **28**, R1 (2002) [arXiv:hep-ph/0107088]
3. A. Bodek, S. Avvakumov, R. Bradford, H. Budd, arXiv: 0709.3538 [hep-ex]
4. K2K Collaboration, R. Gran et al., Phys. Rev. D **74**, 052 002 (2006) [arXiv:hep-ex/0603034]
5. MiniBooNE Collaboration, A.A. Aguilar-Arevalo et al., Phys. Rev. Lett. **100**, 032 301 (2008) [arXiv:0706.0926 [hep-ex]]
6. MiniBooNE Collaboration, T. Katori, AIP Conf. Proc. **967**, 123 (2007) [arXiv:0709.4498 [hep-ex]]
7. P.E. Bosted, Phys. Rev. C **51**, 409 (1995)
8. H. Budd, A. Bodek, J. Arrington, arXiv:hep-ex/0308005
9. R. Bradford, A. Bodek, H. Budd, J. Arrington, Nucl. Phys. Proc. Suppl. **159**, 127 (2006) [arXiv:hep-ex/0602017]
10. R.A. Smith, E.J. Moniz, Nucl. Phys. B **43**, 605 (1972)
11. R.A. Smith, E.J. Moniz, Nucl. Phys. B **101**, 547 (1975) [Erratum]
12. T.B. Novey, Proc. R. Soc. London A **301**, 113 (1967)
13. R.L. Kustom et al., Phys. Rev. Lett. **22**, 1014 (1969)
14. W.A. Mann et al., in: Proceedings of the 16th International Conference on High Energy Physics, National Accelerator Laboratory, Chicago-Batavia, Illinois, September 6–13, 1972, ed. by J.D. Jackson, A. Roberts (National Accelerator Laboratory, Batavia, Illinois, 1973), paper #784
15. W.A. Mann et al., Phys. Rev. Lett. **31**, 844 (1973)
16. ANL-Purdue Collaboration, S.J. Barish et al., preprints COO-1428-428, ANL-HEP-CP-75-38 (unpublished)
17. R.A. Singer, in: Proceedings of the International Conference on Neutrino Physics and Astrophysics, "Neutrino'77", Baksan Valley, USSR, June 18–24, 1977, ed. by M.A. Markov et al. (Publishing office "Nauka," Moscow, USSR, 1978), Vol. 2, p. 95
18. S.J. Barish et al., Phys. Rev. D **16**, 3103 (1977)
19. K.L. Miller et al., Phys. Rev. D **26**, 537 (1982)
20. E.G. Cazzoli et al., in: Proceedings of the International Neutrino Conference, Aachen, West Germany, June 8–12 1976, ed. by H. Faissner, H. Reithler, P. Zerwas (Vieweg, 1977), p. 405
21. E.G. Cazzoli et al., preprint BNL-21677, NG-349, Brookhaven National Laboratory, 1976 (unpublished)
22. A.M. Cnops et al., in: Proceedings of the Topical Conference on Neutrino Physics at Accelerators, Oxford, England, July 4–7, 1978, ed. by A.G. Michette, P.B. Renton (Rutherford Lab, 1978), p. 62
23. A.M. Cnops et al., preprint BNL-24848, OG431, Brookhaven National Laboratory, 1978 (unpublished)
24. G. Fanourakis et al., Phys. Rev. D **21**, 562 (1980)
25. N.J. Baker et al., Phys. Rev. D **23**, 2499 (1981)
26. T. Kitagaki et al., Phys. Rev. D **34**, 2554 (1986)
27. T. Kitagaki et al., in: Proceedings of the International 12th Conference on Neutrino Physics and Astrophysics, "Neutrino'86", Sendai, Japan, June 3–8, 1986, ed. by T. Kitagaki, H. Yuta (World Scientific, 1987), p. 525
28. K. Abe et al., Phys. Rev. Lett. **56**, 1107 (1986)
29. L.A. Ahrens et al., Phys. Rev. D **35**, 785 (1987)
30. L.A. Ahrens et al., Phys. Lett. B **202**, 284 (1988)
31. T. Kitagaki et al., Phys. Rev. D **42**, 1331 (1990)
32. M. Sakuda, in: Proceedings of the 4th International Workshop on Neutrino Oscillations and Their Origin ("NOON 2003"), Kanazawa, Japan, February 10–14, 2003, ed. by Y. Suzuki et al. (World Scientific, River Edge, 2004), p. 253
33. K. Furuno et al., a talk at the 2nd International Workshop on Neutrino–Nucleus Interactions in the few-GeV Region, NuInt'02, University of California, Irvine, December 12–15, 2002, RCNS-03-01, KEK Preprint 2003-48, September, 2003 (unpublished)
34. A.E. Asratyan et al., in: Proceedings of the 12th International Neutrino Conference "Neutrino'82", Balatonfüred, Hungary, June 14–19, 1982, ed. by A. Frenkel, L. Jenik (Central Research Institute of Physics, Budapest, 1982), Supplement Vol. 2, p. 139
35. T. Kitagaki et al., Phys. Rev. D **28**, 436 (1983)
36. A.E. Asratyan et al., Yad. Fiz. **39**, 619 (1984) [Sov. J. Nucl. Phys. **39**, 392 (1984)]
37. A.E. Asratyan et al., Phys. Lett. B **137**, 122 (1984)
38. V.V. Ammosov et al., Pisma. Zh. Eksp. Teor. Fiz. **43**, 554 (1986) [JETP Lett. **43**, 716 (1986)]
39. IHEP-ITEP-MPEI Collaboration, V.V. Ammosov et al., Z. Phys. C **36**, 377 (1987)
40. N. Suwonjandee, PhD Thesis, University of Cincinnati, Cincinnati, 2004, FERMILAB-THESIS-2004-67, Fermi National Accelerator Laboratory, Illinois, 2004 (unpublished), UMI 31-20857
41. H. Burmeister et al., in: Proceedings of the Informal Conference on Experimental Neutrino Physics, CERN, Geneva, January 20–22, 1965, ed. by C. Franzinetti, CERN Yellow Report No. 65-32, European Organization for Nuclear Research, Geneva, 1965, p. 25
42. C. Franzinetti, Lecture given at the Chicago Meeting of the American Physical Society, Chicago, October 28, 1965, CERN Yellow Report No. 66-13, European Organization for Nuclear Research, Geneva, March 1966 (unpublished)
43. E.C.M. Young, PhD Thesis, CERN Yellow Report No. 67-12, European Organization for Nuclear Research, Geneva, 1967 (unpublished)
44. A. Orkin-Lecourtois, C.A. Piketty, Nuovo Cim. A **50**, 927 (1967)
45. M. Holder et al., Nuovo Cim. A **57**, 338 (1968)
46. I. Budagov et al., Lett. Nuovo Cimento **2**, 689 (1969)
47. T. Eichten et al., Phys. Lett. B **40**, 593 (1972)
48. T. Eichten et al., Phys. Lett. B **46**, 274 (1973)
49. F.J. Sciulli, in: Proceedings of the 4th International Conference on Neutrino Physics and Astrophysics "Neutrino'74", Downigtown, Pennsylvania, April 26–28, 1974, ed. by C. Baltay, AIP Conf. Proc. **22**, 166 (1974)
50. Aachen-Brussels-CERN-Paris-Milano-Orsay-London Collaboration, M. Haguenauer, in: Proceedings of the 17th International Conference on High Energy Physics, London, July 1–10, 1974, ed. by J.R. Smith (Rutherford High Energy Laboratory, Didcot, Berkshire, England, 1975), p. IV-95
51. Aachen-Bruxelles-CERN-Ecole Polytechnique-Orsay-London Collaboration, M. Rollier, in: Proceedings of the International Colloquium on High Energy Neutrino Physics,

Paris, France, March 18–20, 1975, (Editions du CNRS, École Polytechnique, 1975), p. 349
52. Gargamelle Neutrino Collaboration, H. Deden et al., Nucl. Phys. B **85**, 269 (1975)
53. S. Bonetti et al., Nuovo Cim. A **38**, 260 (1977)
54. O. Erriquez et al., Phys. Lett. B **70**, 383 (1977)
55. Gargamelle Antineutrino Collaboration, Bari-Milano-Strasbourg-Torino-University College London, M. Rollier, in: Proceedings of the Topical Conference on Neutrino Physics at Accelerators, Oxford, England, July 4–7, 1978, ed. by A.G. Michette, P.B. Renton (Rutherford Lab, 1978), p. 68
56. Aachen-Bruxelles-CERN-Ecole Polytechnique-Orsay-Padova Collaboration, M. Dewit, in: Proceedings of the Topical Conference on Neutrino Physics at Accelerators, Oxford, England, July 4–7, 1978, ed. by A.G. Michette, P.B. Renton (Rutherford Lab, 1978), p. 75
57. O. Erriquez et al., Nucl. Phys. B **140**, 123 (1978)
58. Gargamelle Neutrino Propane Collaboration, M. Pohl et al., Lett. Nuovo Cimento **26**, 332 (1979)
59. N. Armenise et al., Nucl. Phys. B **152**, 365 (1979)
60. Amsterdam-Bergen-Bologna-Padova-Pisa-Saclay-Torino Collaboration, D. Allasia et al., Nucl. Phys. B **343**, 285 (1990)
61. NOMAD Collaboration, R. Petti, in: Proceedings of 32nd International Conference on High-Energy Physics (ICHEP'04), Beijing, China, August 16–22, 2004, ed. by H. Chen, D. Du, W. Li, C. Lu (Hackensack, World Scientific, 2005), Vol. **1**, p. 468 [arXiv:hep-ex/0411032]
62. V.V. Lyubushkin, B.A. Popov, Yad. Fiz. **69**, 1917 (2006) [Phys. Atom. Nucl. **69**, 1876 (2006)]
63. A. Martinez de la Ossa Romero, arXiv:hep-ex/0703026
64. V.V. Lyubushkin, PhD Thesis, JINR, Dubna, 2008 (unpublished)
65. V.V. Makeev et al., Pisma. Zh. Eksp. Teor. Fiz. **34**, 418 (1981) [JETP Lett. **34**, 397 (1981)]
66. IHEP-ITEP Collaboration, S.V. Belikov et al., preprint IFVE 81-146 ONF SERP-E-45, Serpukhov, 1981 (unpublished)
67. S.V. Belikov et al., preprint IFVE 82-107 ONF SERP-E-45, Serpukhov, 1982 (unpublished)
68. S.V. Belikov et al., Yad. Fiz. **35**, 59 (1982) [Sov. J. Nucl. Phys. **35**, 35 (1982)]
69. S.V. Belikov et al., Pisma. Zh. Eksp. Teor. Fiz. **38**, 547 (1983) [JETP Lett. **38**, 661 (1983)]
70. S.V. Belikov et al., Yad. Fiz. **41**, 919 (1985) [Sov. J. Nucl. Phys. **41**, 589 (1985)]
71. S.V. Belikov et al., Z. Phys. A **320**, 625 (1985)
72. SKAT Collaboration, H.J. Grabosch et al., preprints PHE 86-11, Berlin-Zeuthen, 1986 and IFVE 86-221 ONF SERP-E-107, Serpukhov, 1986 (unpublished)
73. H.J. Grabosch et al., Yad. Fiz. **47**, 1630 (1988) [Sov. J. Nucl. Phys. **47**, 1032 (1988)]
74. SKAT Collaboration, J. Brunner et al., Z. Phys. C **45**, 551 (1990)
75. A. Bodek, S. Avvakumov, R. Bradford, H. Budd, Eur. Phys. J. C **53**, 349 (2008) [arXiv:0708.1946 [hep-ex]]
76. A. Bodek, S. Avvakumov, R. Bradford, H. Budd, arXiv: 0708.1827 [hep-ex]
77. E.L. Lomon, arXiv:nucl-th/0609020
78. A. Strumia, F. Vissani, Phys. Lett. B **564**, 42 (2003) [arXiv:astro-ph/0302055]
79. K.S. Kuzmin, V.V. Lyubushkin, V.A. Naumov, Nucl. Phys. B Proc. Suppl. **139**, 154 (2005) [arXiv:hep-ph/0408107]
80. K.S. Kuzmin, V.V. Lyubushkin, V.A. Naumov, Acta Phys. Pol. B **37**, 2337 (2006) [arXiv:hep-ph/0606184]
81. C.H. Llewellyn Smith, Phys. Rep. **3**, 261 (1972)
82. D.H. Wilkinson, Eur. Phys. J. A **7**, 307 (2000)
83. D.H. Wilkinson, Nucl. Instrum. Methods A **456**, 655 (2000)
84. D.H. Wilkinson, Nucl. Instrum. Methods A **469**, 286 (2001)
85. S. Gardner, C. Zhang, Phys. Rev. Lett. **86**, 5666 (2001) [arXiv:hep-ph/0012098]
86. J.J. Kelly, Phys. Rev. C **70**, 068 202 (2004)
87. M.F. Gari, W. Krüempelmann, Phys. Lett. B **274**, 159 (1992)
88. M.F. Gari, W. Krüempelmann, Phys. Lett. B **282**, 483(E) (1992)
89. E.L. Lomon, Phys. Rev. C **64**, 035 204 (2001) [arXiv: nucl-th/0104039]
90. E.L. Lomon, Phys. Rev. C **66**, 045 501 (2002) [arXiv: nucl-th/0203081]
91. J. Arrington, Phys. Rev. C **68**, 034 325 (2003) [arXiv: nucl-ex/0305009]
92. J. Arrington, Eur. Phys. J. A **17**, 311 (2003) [arXiv: hep-ph/0209243]
93. JLab E93-038 Collaboration, J.M. Finn, Fizika B **13**, 545 (2004)
94. Jefferson Lab E95-001 Collaboration, B. Anderson et al., Phys. Rev. C **75**, 034 003 (2007) [arXiv:nucl-ex/0605006]
95. D. Day, Eur. Phys. J. A **31**, 560 (2007)
96. C.F. Perdrisat, V. Punjabi, M. Vanderhaeghen, Prog. Part. Nucl. Phys. **59**, 694 (2007) [arXiv:hep-ph/0612014]
97. K. Hagiwara, K. Mawatari, H. Yokoya, Phys. Lett. B **591**, 113 (2004) [arXiv:hep-ph/0403076]
98. K.S. Kuzmin, V.V. Lyubushkin, V.A. Naumov, Mod. Phys. Lett. A **19**, 2919 (2004) [arXiv:hep-ph/0403110]
99. Particle Data Group, W.M. Yao et al., J. Phys. G **33**, 1 (2006)
100. D. Pocanic et al., Phys. Rev. Lett. **93**, 181 803 (2004) [arXiv:hep-ex/0312030]
101. S. Nakamura et al., Nucl. Phys. A **707**, 561 (2002) [arXiv:nucl-th/0201062]
102. D.H. Perkins, in: Proceedings of the 16th International Conference on High Energy Physics, National Accelerator Laboratory, Chicago-Batavia, Illinois, September 6–13, 1972, ed. by J.D. Jackson, A. Roberts (National Accelerator Laboratory, Batavia, Illinois, 1973), Vol. **IV**, p. 189
103. M. Derrick, in: Proceedings of the 17th International Conference on High Energy Physics, London, July 1–10, 1974, ed. by J.R. Smith (Rutherford High Energy Laboratory, Didcot, Berkshire, England, 1975), p. II-166
104. D.H. Perkins, in: Proceedings of the 1975 International Symposium on Lepton and Photon Interactions at High Energies, Stanford University, August 21–27, 1975, ed. by T.W. Kirk (Stanford Linear Accelerator Center, Stanford, 1975), p. 571
105. D. Cline, W.F. Fry, Ann. Rev. Nucl. Part. Sci. **27**, 209 (1977)
106. H. Wachsmuth, "Accelerator neutrino physics", Lectures held at the Herbstschule für Hochenergiephysik, Maria Laach, Eifel, Germany, September 14–24, 1976, preprint CERN/EP/PHYS 77-40, August 17, 1977 (unpublished)
107. P.F. Ermolov, A.I. Mukhin, Usp. Fiz. Nauk. **124**, 385 (1978) [Sov. Phys. Uspekhi **21**, 185 (1978)]
108. P. Musset, J.-P. Vialle, Phys. Rep. **39**, 1 (1978)

109. S.I. Alekhin et al., Report CERN-HERA 87-01, European Organization for Nuclear Research, Geneva, 1987
110. M. Sakuda, Nucl. Phys. B Proc. Suppl. **112**, 109 (2002)
111. V.V. Ammosov et al., Fiz. Elem. Chast. Atom. Yadra **23**, 648 (1992) [Sov. J. Part. Nucl. **23**, 283 (1992)]
112. C. Baltay, Nucl. Phys. B Proc. Suppl. **36**, 363 (1994)
113. G.P. Zeller, a talk at the 2nd International Workshop on Neutrino-Nucleus Interactions in the few-GeV Region, NuInt'02, University of California, Irvine, December 12–15, 2002 [arXiv:hep-ex/0312061]
114. B. Fleming, AIP Conf. Proc. **815**, 1 (2006)
115. M. Sorel, AIP Conf. Proc. **967**, 17 (2007) [arXiv:0710.3966 [hep-ex]]
116. R. Gran, AIP Conf. Proc. **967**, 141 (2007) [arXiv:0711.3024 [hep-ex]]
117. F. James, "MINUIT, Reference Manual, Version 94.1", CERN Program Library Long Writeup D506 (European Organization for Nuclear Research, Geneva, 1994)
118. F. James, M. Roos, Comput. Phys. Commun. **10**, 343 (1975)
119. I. Budagov et al., Phys. Lett. B **29**, 524 (1969)
120. Amsterdam-Bergen-Bologna-Padova-Pisa-Saclay-Torino Collaboration, D. Allasia et al., Nucl. Phys. B **239**, 301 (1984)
121. S.K. Singh, Nucl. Phys. B **36**, 419 (1972)
122. N.J. Baker et al., Phys. Rev. D **28**, 2900 (1983)
123. A.V. Butkevich, S.P. Mikheyev, Phys. Rev. C **72**, 025 501 (2005) [arXiv:hep-ph/0505008]
124. A.V. Butkevich, S.A. Kulagin, Phys. Rev. C **76**, 045 502 (2007) [arXiv:0705.1051 [nucl-th]]
125. K.S. Kuzmin, V.V. Lyubushkin, V.A. Naumov, Yad. Fiz. **69**, 1898 (2006) [Phys. Atom. Nucl. **69**, 1857 (2006)] [arXiv:hep-ph/0511308]
126. K2K Collaboration, M.H. Ahn et al., Phys. Rev. Lett. **93**, 051 801 (2004) [arXiv:hep-ex/0402017]
127. K2K Collaboration, M.H. Ahn et al., Phys. Rev. D **74**, 072 003 (2006) [arXiv:hep-ex/0606032]
128. Super-Kamiokande Collaboration, Y. Ashie et al., Phys. Rev. D **71**, 112 005 (2005) [arXiv:hep-ex/0501064]